

RECENT PHYSICS RESULTS FROM CDF AND D0

Evelyn J. Thomson*
Department of Physics
The Ohio State University
174 West 18th Ave.
Columbus, OH 43210

Representing the CDF and D0 Collaborations

ABSTRACT

Recent physics results from CDF and D0 on heavy flavor physics, electroweak precision measurements, top physics, QCD and searches for new physics are discussed. The results are based on approximately 140 pb^{-1} of data collected at $\sqrt{s}=1.96\text{ TeV}$ between 2002 and 2003.

*Supported by DOE Contract DE-FG02-91ER40690.

1 Introduction

The CDF and D0 detectors are general, multi-purpose experiments run by international collaborations, each with over 700 participants, at the Fermilab Tevatron accelerator, which now collides protons and anti-protons at $\sqrt{s}=1.96$ TeV. This is the highest energy available at a collider facility until the CERN LHC starts up in 2007 at $\sqrt{s}=14$ TeV. Previous results from CDF and D0 were based on about 100 pb^{-1} of data collected at $\sqrt{s}=1.8$ TeV from 1989 to 1995. Both the detectors and the accelerator have since been upgraded and data-taking resumed in 2001. CDF and D0 expect to cross the 2000 pb^{-1} threshold by 2007 and to accumulate 4000-9000 pb^{-1} by 2009.

Recent physics results from CDF and D0, based on approximately 140 pb^{-1} of new data, further expand our knowledge in several areas of high energy physics:

- **Heavy Flavor Physics:** The charm quark, discovered in 1974, and the bottom quark, discovered in 1977, still have some secrets left, most notably the mixing frequency of the B_s meson. The e^+e^- B-factories, BABAR and BELLE, at the $\Upsilon(4S)$ resonance are dedicated to the study of the B_d and B_u mesons, so CDF and D0 are now the only running experiments that can study the properties of the other B mesons and baryons. A novel trigger strategy, based on the long lifetimes of the bottom and charm hadrons, has been successfully implemented by CDF to take advantage of the large heavy flavor production cross-section. Recent results include the production cross-section of several charm mesons and the mass, lifetime, branching fractions and CP asymmetries of B hadrons.
- **Electroweak Physics:** The Z and W bosons were discovered by UA1 and UA2 in 1983. The properties of the Z boson have been measured very precisely already by the LEP experiments and SLD. The W boson mass is fundamental to precision tests of the Standard Model. With over 2 million reconstructed $W \rightarrow \ell\nu$ decays, where $\ell = e, \mu$, in 2000 pb^{-1} , CDF and D0 expect to measure the W boson mass with a precision of $40\text{ MeV}/c^2$, independent of and comparable to the best measurement of the W boson mass from the LEP experiments. Recent results include the W and Z production cross-sections, the W width and the forward-backward asymmetry of e^+e^- pairs.
- **Top Physics:** The top quark, the sixth and final quark in the Standard

Model, was discovered in 1995 by CDF and D0. The surprisingly large top quark mass of $m_t = 174.3 \pm 5.1 \text{ GeV}/c^2$ - more than 35 times heavier than the b quark and almost as massive as a gold atom - means that the Tevatron is the only running accelerator with enough energy to produce top quarks. The increase in the Tevatron \sqrt{s} from 1.8 TeV to 1.96 TeV is strongly motivated by the expected 30% increase in the top production cross-section. The top quark mass is fundamental to precision tests of the Standard Model and especially to the bound on the Standard Model Higgs boson mass - an important goal of CDF and D0 is to reduce the uncertainty on the top quark mass below $3 \text{ GeV}/c^2$ with 2000 pb^{-1} . The puzzle of why the top quark mass is so much larger than the other quarks has provided fertile ground for many theories beyond the Standard Model. Measurements of other properties of the top quark could provide surprising answers. Recent results include the top pair production cross-section, the top quark mass and limits on the single top production cross-section.

- **QCD:** Measurements of jet production test the predictions of NLO QCD to the highest energies and thus probe the structure of the proton to the smallest distances yet, of order 10^{-19} m . In particular, improved knowledge of the parton density functions of the proton is essential to clearly identify effects from new physics. Comparisons of W+jet and Z+jet production with new and improved models are important as a test of QCD at high momentum transfers and since W+jet production is the dominant background for Top physics and to the search for the Standard Model Higgs boson. Detailed understanding of jet reconstruction algorithms is also important to all other physics measurements involving jets, especially the top mass measurement. Recent results include inclusive jet and dijet mass cross-section measurements.
- **Searches for New Physics:** Recent advances in cosmology discussed at this summer school, especially the results from WMAP,⁷ show that particles in the Standard Model only account for 4% of the energy density in the universe whereas the mysterious dark matter makes up 22%. So there is much more left to search for than just the Standard Model Higgs boson. Indeed, some of the models beyond the Standard Model provide attractive candidates for this dark matter, linking the very large scales of cosmology to the very small scales

of particle physics. Direct searches for new particles and effects predicted by the many models beyond the Standard Model will either yield the world's best limits or evidence for new physics. Recent results include searches for models with extra dimensions, extra gauge bosons, leptoquarks and SUSY.

While I will do my best to review such a bounty of results in so little space-time, I recommend the interested reader to explore the public web pages of CDF¹ and D0² for more details and the latest results. The presentations at and the proceedings from the 2003 EPS³ and Lepton-Photon⁴ conferences are also a valuable resource. I will begin by discussing the environment for physics at a hadron collider, with information on the CDF and D0 detectors and the recent performance of the accelerator. Following the regions of interest listed above, I will summarize recent physics results from CDF and D0 in the next five sections.

2 The Hadron Collider Environment

Doing physics at a hadron collider is like panning for gold under Niagara Falls. At the Tevatron, there are 1.7 million collisions per second between bunches of protons and anti-protons at the centre of each detector. On every collision, usually at least one proton and anti-proton interacts with hard scattering between a pair of their constituent partons (quarks, anti-quarks and gluons) to create tens of particles that leave measurable signals in the detector - a very busy environment! There are many different physics processes by which the partons can interact. The most common processes are already well understood, so it is the rarer processes that are of interest to the current physics programs of CDF and D0. To give you a sense of what rare means, Table 1 compares the cross-section of some physics processes and their event rate at the Tevatron. Fewer than one in a million collisions produces a W or Z vector boson and fewer than one in a billion collisions produces a pair of top and anti-top quarks.

Information from the detector can be permanently saved for later physics analysis at an average rate of about 10 Megabytes per second. With the complete detector readout for one collision weighing in at roughly 150 kilobytes, only 70 of the 1.7 million collisions per second can be saved. This means that we must reject about 25,000 other collisions forever for each collision we keep and we must decide very fast - at the bunch crossing frequency! With event rates already so

Process	Cross-section	Event Rate
Inelastic $p\bar{p}$	60 mb	6 MHz
$p\bar{p} \rightarrow b\bar{b}$ (b $p_T > 6$ GeV, $ \eta < 1$)	10 μ b	1 kHz
$p\bar{p} \rightarrow W + X \rightarrow \ell\nu + X$	5 nb	0.5 Hz
$p\bar{p} \rightarrow Z + X \rightarrow \ell^+ \ell^- + X$	0.5 nb	0.05 Hz
$p\bar{p} \rightarrow t\bar{t} + X \rightarrow W^+ b W^- \bar{b} + X \rightarrow \ell\nu q\bar{q} b\bar{b} + X$	2 pb	0.0002 Hz
$p\bar{p} \rightarrow WH \rightarrow \ell\nu b\bar{b}$ (if $M_H = 120$ GeV/ c^2)	15 fb	0.0000015 Hz

Table 1: Cross-section of some physics processes at the Fermilab Tevatron with $\sqrt{s}=1.96$ TeV. The event rate is the cross-section multiplied by the instantaneous luminosity, assumed here to be $100 \times 10^{30} \text{cm}^{-2}\text{s}^{-1}$. ℓ indicates an electron or muon.

low for top and electroweak physics, we obviously cannot afford to discard events from these processes and it is therefore critical to be able to identify and keep these rare events with high efficiency. In contrast, the event rates are much higher than 70 Hz for QCD and B physics, so the challenge here is to use the available bandwidth as intelligently as possible to keep the most interesting events.

Fortunately, the interesting processes have characteristic signatures that the detectors are designed to recognize:

- **High Transverse Energy.** Remember that the probability distribution for the fraction of the proton's momentum, x , carried by a particular parton peaks towards zero. Therefore, the most common interactions occur between low energy partons and thus the jets of hadronic particles produced have low energy relative to the proton beam energy. However, the production of such massive objects as W and Z bosons and top quarks obviously requires the colliding partons to carry a significant fraction of the parent proton/anti-proton momentum and thus their decay products are very energetic. Since the longitudinal boost of a particular interaction is unknown, only the energy transverse to the beam direction is useful for discrimination.
- **Leptons.** While the decays of vector bosons to quarks still closely resemble the more common QCD multi-jet production, the decays to leptons with high transverse energy give very distinctive signatures that are easy to identify with very high efficiency. Decays of bottom and charm hadrons can produce

leptons with lower transverse energy. At these lower energies, muons are easier to pick out than electrons since photon conversions in detector material also produce lots of electrons and the measurement of the electron momentum is degraded by bremsstrahlung.

- **Missing Transverse Energy.** The presence of neutrinos or more exotic neutral particles that escape the detector intact is inferred by an imbalance in the total observed transverse energy. Note the finite calorimeter resolution as well as incomplete calorimeter coverage can cause events with neither neutrinos nor anything more exotic to have significant missing transverse energy.
- **Displaced tracks and vertices.** The long lifetimes of the beauty and charm hadrons mean that these particles typically travel about 1-2 mm before decaying into several secondary particles. The compact size of the beam in the transverse direction ($30\text{ }\mu\text{m}$) and the precision of the spatial information from the silicon microstrip subdetectors is such that the displacement of the reconstructed tracks of the charged secondaries with respect to the primary interaction point is resolvable.

The trick to doing this fast enough and therefore the key to physics at a hadron collider is called the trigger - the sophisticated hybrid of hardware and software that processes the detector readout from every bunch crossing (“all of Niagara Falls”) to select the interesting events (“gold”) for later analysis. Both CDF and D0 employ three level trigger systems, with each successive level using more refined information to apply more stringent selection criteria. For instance at CDF, the Level 1 trigger uses custom hardware to identify charged particle tracks, electrons, muons and clusters of energy in the calorimeters to reduce the rate from the 1.7 MHz bunch crossing frequency to 30 kHz. The Level 2 trigger adds more information to find displaced tracks, jets, photons and improve the definition of electrons and muons to further reduce the rate to 300 Hz. The Level 3 trigger uses a farm of 300 Linux PCs running a streamlined version of the physics analysis reconstruction to filter out the 70 Hz that can be written to permanent storage.

The CDF detector,⁸ shown in Figure 1, now has a completely new charged particle tracking system inside the 1.4 T axial magnetic field from the original superconducting solenoid. The main tracking subdetector (COT) is again a wire drift

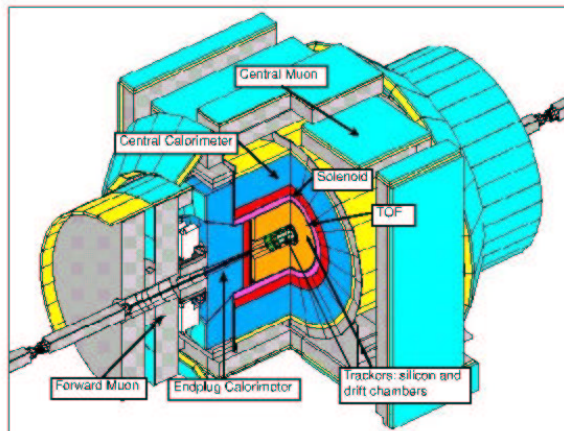


Figure 1: The upgraded CDF detector for Run II.

chamber but with a much smaller cell size of about 0.88 cm so that the maximum drift time is less than the time between bunch crossings. The 96 layers of wires between 44 and 132 cm in radius provide 2D space-points with a resolution of about $180\ \mu\text{m}$ and also dE/dx information for proton-pion-kaon particle identification. The layers are grouped radially into 8 superlayers of 12 wires each, four superlayers are slightly offset to provide stereo information for 3D track reconstruction. A double-sided five-layer silicon subdetector (SVX) provides precise 3D space-points, with a resolution of about $12\ \mu\text{m}$, between 2.5 and 10.6 cm in radius and extends much further than the Run I detector in z to ± 48 cm in order to cover most of the luminous region. A double-sided two-layer silicon subdetector (ISL) at radii of 20 and 28 cm provides additional precise 3D space-points to make silicon-only tracking possible for $|\eta| \leq 2.0$. A single-sided layer of silicon (L00) mounted directly on the beampipe at a radius of about 1.5 cm further improves the impact parameter resolution to extend the reach of the B_s mixing analysis. The full tracking system provides an excellent momentum resolution of $\frac{\Delta p_T}{p_T} = 0.007 \oplus 0.001 p_T$ and an impact parameter resolution of $\Delta d_0[\mu\text{m}] = 6 \oplus 22/p_T(\text{GeV})$. A time-of-flight subdetector (TOF) fits neatly into the space between the COT and the superconducting solenoid to provide good pion-kaon separation for $p_T < 1.6\ \text{GeV}/c$. Outside the solenoid, calorimeters cover the region out to $|\eta| < 3.6$ and measure the energy of electrons and photons with a resolution of $16/\sqrt{E}\%$ and hadronic jets with a resolution of $80/\sqrt{E}\%$. The calorimeter between 1.1 and 3.6 in $|\eta|$ has been replaced and is now a Pb-scintillator (EM) and Fe-scintillator (HAD) sandwich much like the retained central calorimeter. Inside the EM calorimeter,

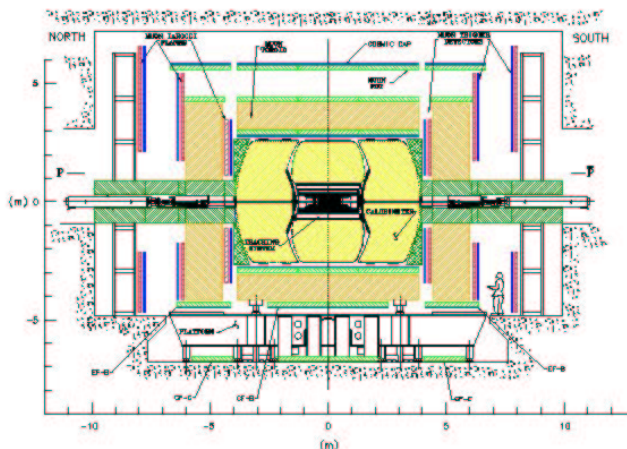


Figure 2: The upgraded D0 detector for Run II.

fine-grained shower profile detectors at the electromagnetic shower maximum distinguish between electromagnetic and hadronic showers. Outside the calorimeters, the coverage of the muon chambers has been extended to cover $1.0\text{--}1.5$ in $|\eta|$ and to increase the azimuthal coverage to above 80%. The readout electronics for all the subdetectors as well as the trigger and data acquisition systems have been totally replaced in order to operate at the shortest proposed bunch crossing time for the accelerator of 132 ns. For the first time, CDF has the capability in the trigger at Level 1 to reconstruct charged particle tracks in the central drift chamber with p_T above 1.5 GeV/c, with a p_T resolution of better than 2%/GeV/c and azimuthal resolution better than 8 mrad. In addition, the Level 2 trigger adds silicon hits to find displaced tracks with an impact parameter resolution of 48 μm (convolution of 35 μm intrinsic resolution and 33 μm from the beam transverse width). Combined with the large bandwidth inherent to the CDF trigger design, this allows CDF to collect large samples of low p_T hadronic B decays.

The D0 detector,⁹ shown in Figure 2, retains the uranium liquid-argon sampling calorimeter that extends out to $|\eta| = 4$ with fine longitudinal and transverse segmentation, $\Delta\eta \times \Delta\phi = 0.1 \times 0.1$. The calorimeter energy resolution is $15/\sqrt{E}\%$ for electrons and photons and $80/\sqrt{E}\%$ for hadronic jets. The design of the new D0 tracking system is optimized for the small lever arm of 52 cm available within the calorimeter. For the first time, the D0 tracking subdetectors are immersed in an axial magnetic field of 2.0 T from a superconducting solenoid. There are 4 double-sided layers of silicon between 2.8 and 10.0 cm in radius in the central region covering $|z| < 32$ cm and several disks of silicon at larger z to extend the

tracking acceptance out to $|\eta| < 3$. The eight layer scintillating fiber tracker between 20 and 52 cm provides 2D space-points with a resolution of about $100 \mu\text{m}$. One of the two doublets of fibers in each layer is slightly offset to provide stereo information for 3D track reconstruction. The full tracking system provides a momentum resolution of $\frac{\Delta p_T}{p_T} = 0.02 \oplus 0.002 p_T$ and an impact parameter resolution of $\Delta d_0[\mu\text{m}] = 13 \oplus 50/p_T(\text{GeV})$. A new scintillating strip pre-shower subdetector mounted on the inner surface of the calorimeter cryostats provides finer spatial information to better distinguish between electromagnetic showers and hadronic showers given the increased material in the inner detector. Outside the calorimeter, the muon system extends to 2.0 in $|\eta|$ and the azimuthal coverage is over 90%. The forward muon system $|\eta| > 1$ has been completely replaced. The read-out electronics for all subdetectors and the trigger and data acquisition systems have been totally replaced. D0 also has a Level 1 track trigger and is currently commissioning a displaced track trigger at Level 2. Note the maximum Level 1 accept rate is 5 kHz, so D0 will not be able to support a CDF-like high bandwidth Level 1 trigger for hadronic B decays.

The Fermilab Tevatron proton-antiproton collider was originally designed and constructed in the 1980's to mass produce W and Z bosons. Several upgrades have been made to enhance the performance of the accelerator complex in order to provide the higher luminosities required to achieve the goals of the CDF and D0 Run II physics programs in a relatively short amount of time.⁵ The recent performance of the Fermilab Tevatron Collider is shown in Figure 3. The recent initial instantaneous luminosity of around $40 \times 10^{30} \text{ cm}^{-2}\text{s}^{-1}$ is over a factor of two higher than the Run I best of $16 \times 10^{30} \text{ cm}^{-2}\text{s}^{-1}$. This is mainly due to the new Main Injector which allows larger numbers of protons to be accelerated from 8 GeV to 150 GeV for injection into the Tevatron and also to 120 GeV for antiproton production. Another factor of two increase in the initial instantaneous luminosity is expected over the next year from targeted improvements to several limiting factors for anti-proton production and the number of protons delivered to the experimental interaction regions.⁶ Improving the operational stability of the accelerator complex will also be important in order for the experiments to accumulate large integrated luminosities. The integrated luminosity delivered to the experiments in the past year is about 200 pb^{-1} , with about 350 pb^{-1} expected in the next year.

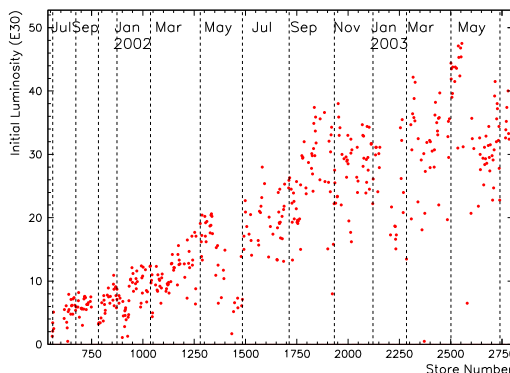


Figure 3: Initial instantaneous luminosity versus time of the Fermilab Tevatron collider in Run II.

3 Heavy Flavor Physics

With the beautiful results¹⁰ from BABAR and BELLE on the properties of the B_d and B_u mesons, I have concentrated on showing what CDF and D0 can add with studies of charm physics, the B_s meson and the Λ_b baryon. Note, specific triggers are used to select these heavy flavor decay modes:

- B and D decays with a $J/\psi \rightarrow \mu^+\mu^-$: both CDF and D0 can trigger on events with two muons down to a very low momentum of $p_T > 1.5$ GeV/c.
- Semi-leptonic B and D decays: D0 has inclusive lepton triggers with excellent acceptance, CDF has a lepton + displaced track trigger to provide cleaner samples where typical requirements are lepton $p_T > 4$ GeV/c, track $p_T > 2$ GeV/c and $d_0 > 120$ μm .
- Hadronic B and D decays: CDF has a displaced two track trigger where typical requirements are track $p_T > 2$ GeV/c, $d_0 > 120$ μm , $\Delta\phi < 135^\circ$ and $\Sigma p_T > 5.5$ GeV/c.

3.1 D Meson Mass Difference

The CDF measurement of the mass difference between the D_s^+ and D^+ mesons* is the first publication from the Tevatron in Run II.¹¹ The data sample is collected with the new displaced two-track trigger. The analysis uses a common final decay

*Unless otherwise specified, the charge conjugate modes are also implied throughout this note.

state of $\phi\pi^+$, where the ϕ decays to two charged kaons. No particle identification is used, instead advantage is taken of the very narrow ϕ resonance and the excellent mass resolution of the CDF spectrometer. A ϕ meson candidate is a pair of oppositely charged tracks, assumed to be kaons, with an invariant mass within 10 MeV/c² of the world average¹² ϕ mass. The detector resolution on the ϕ mass is 4 MeV/c². A third track, assumed to be a pion, is then added and all three tracks are constrained to be from a common vertex.

The mass of the D meson candidate depends on the measured momenta of its decay products, so it is important to calibrate the momentum scale. A sample of 55,000 $J/\psi \rightarrow \mu^+\mu^-$ decays is used to understand the momentum scale. Ideally, the measured J/ψ mass shown in Figure 4 should be constant with the J/ψ p_T . After removing the p_T dependence by correcting the track fits for energy losses in the detector material, the magnetic field strength used to convert track curvature to momentum is calibrated by comparing the observed mass to the world average

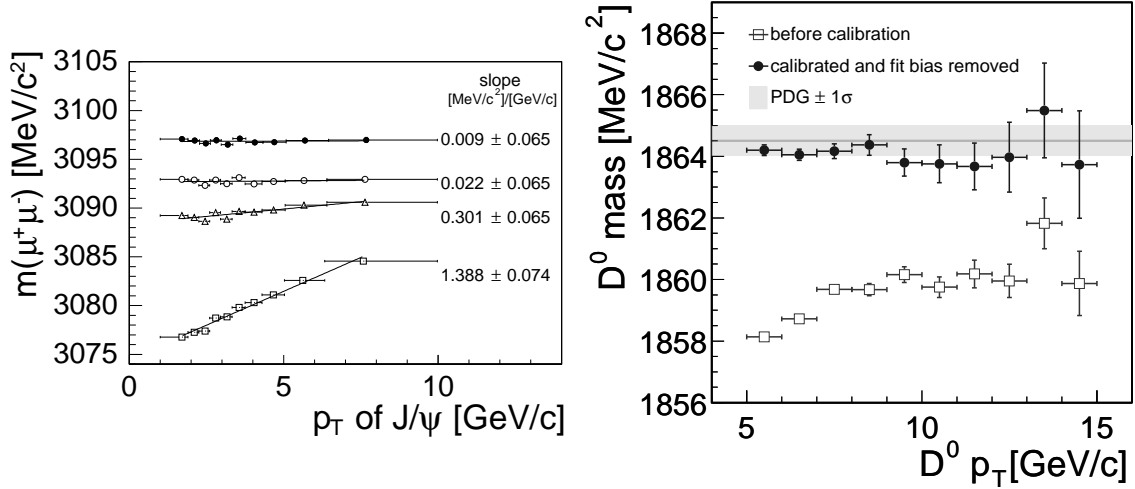


Figure 4: The dependence of the J/ψ mass on the p_T of the J/ψ is shown on the left. The open squares show the mass dependence for tracks with no energy loss corrections. Open triangles show the result after applying the energy loss correction for material in the GEANT description of the detector. Open circles are after accounting for extra material missing in that GEANT description. Filled circles are after the B field tuning. The dependence of the D^0 mass on the p_T of the D^0 meson is shown on the right, before and after the calibration developed with the J/ψ events.

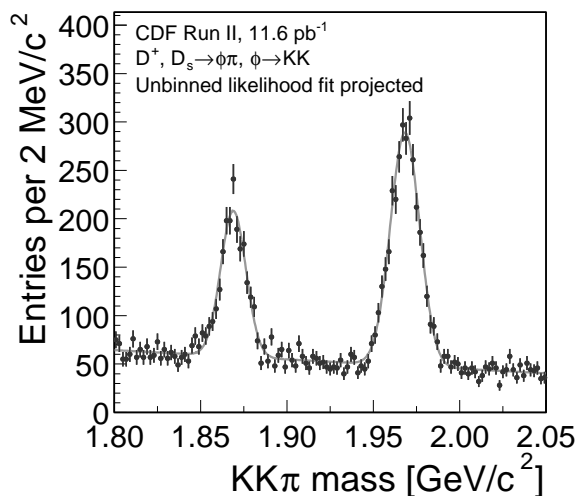


Figure 5: Measured $K^+K^-\pi^+$ mass distribution compared to the unbinned likelihood fit of two Gaussians and a linear background.

value. This calibration prescription is then tested with low momentum pions from $K_s \rightarrow \pi^+\pi^-$, high momentum muons from $\Upsilon \rightarrow \mu^+\mu^-$ and with kaons and pions from $D^0 \rightarrow K^+\pi^-$ decays, shown in Figure 4. All CDF heavy flavor analysis discussed in this review use this calibration procedure.

The almost identical kinematics of D_s^+ and D^+ meson decays to $\phi\pi^+$ mean many systematics cancel in the mass difference, which is shown in Figure 5 and measured to be $99.41 \pm 0.38(stat) \pm 0.21(sys)$ MeV/ c^2 with $11.6 pb^{-1}$. This agrees well with the world average of 99.5 ± 0.50 MeV/ c^2 and to a recent result from BABAR¹³ of $98.4 \pm 0.1(stat) \pm 0.3(sys)$ MeV/ c^2 . Note that only a small fraction of the CDF Run II data was used for this result. With a factor of 20 more statistics already collected, this measurement will soon be able to narrow the range of parameters and assumptions that theoretical models use to make predictions.

3.2 Prompt Charm Meson cross-section

Previously published measurements of the b production cross-section at the Tevatron have consistently been significantly higher than the predictions from Next-to-Leading Order QCD. CDF has made the first measurement of the charm production cross-section¹⁴ at a hadron collider using a large sample of charm decays collected using the new displaced track trigger.

Meson	Momentum range (GeV/c)	Measured cross-section (μb)
D^0	$p_T > 5.5$	$13.3 \pm 0.2 \pm 1.5$
D^{*+}	$p_T > 6.0$	$5.2 \pm 0.1 \pm 0.8$
D^+	$p_T > 6.0$	$4.3 \pm 0.1 \pm 0.7$
D_s^+	$p_T > 8.0$	$0.75 \pm 0.05 \pm 0.22$

Table 2: The measured cross-section for prompt charm mesons with $|y| < 1$.

Since the events are accepted based upon daughter tracks with large impact parameter, it is clear that the sample of reconstructed charm decays contains charm from bottom decays in addition to prompt charm production. The fraction of charm mesons coming from prompt production is measured to be 80-90% (depending on the mode) using the impact parameter of the charm meson - charm mesons from $c\bar{c}$ production have a small impact parameter pointing back to the primary vertex, whereas charm mesons from b decays have a larger impact parameter that may not point back to the primary vertex due to the transverse momentum kick from the b decay.

The charm meson cross-sections are measured in the central rapidity region $|y| \leq 1$ in four fully reconstructed decay modes: $D^0 \rightarrow K^-\pi^+$, $D^{*+} \rightarrow D^0\pi^+$ with $D^0 \rightarrow K^-\pi^+$, $D^+ \rightarrow K^-\pi^+\pi^+$, $D_s^+ \rightarrow \phi\pi^+$ with $\phi \rightarrow K^+K^-$ and their charge conjugates. The integrated cross-section results are shown in Table 2. The measured differential cross-section is compared with the prediction from NLO QCD¹⁵ in Figure 6. The predicted cross-section seems to model the shape well, but is lower than the measured results. This makes interpretations that ascribe the difference in the B meson cross-sections to new physics beyond the Standard Model less likely.

3.3 Mass and Lifetime of the B_s meson

These B_s meson analysis use the fully reconstructed $J/\psi\phi$ decay mode, where $J/\psi \rightarrow \mu^+\mu^-$ and $\phi \rightarrow K^+K^-$. The data sample is collected with a di-muon trigger. The ϕ meson candidate is a pair of oppositely charged tracks, assumed to be kaons, with an invariant mass close to the world average. The J/ψ and ϕ meson candidates are constrained to come from a common vertex. Similar final states with higher statistics from the $B^+ \rightarrow J/\psi K^+$ and $B^0 \rightarrow J/\psi K^{*0}$ decays

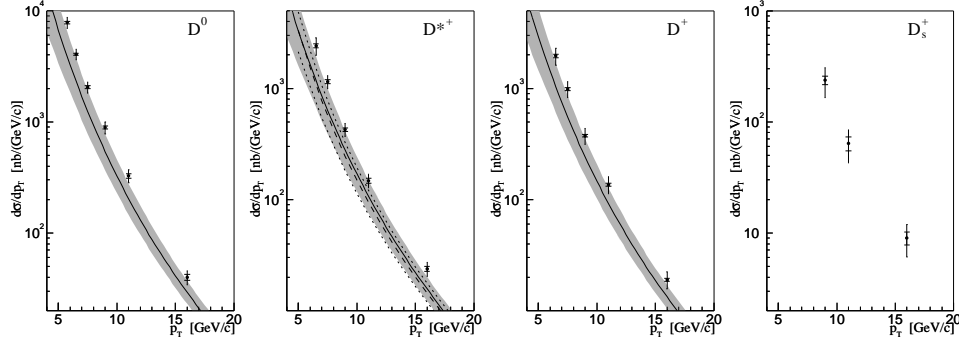


Figure 6: The measured differential cross-section for prompt charm mesons with $|y| < 1$ compared to the prediction from NLO QCD.¹⁵

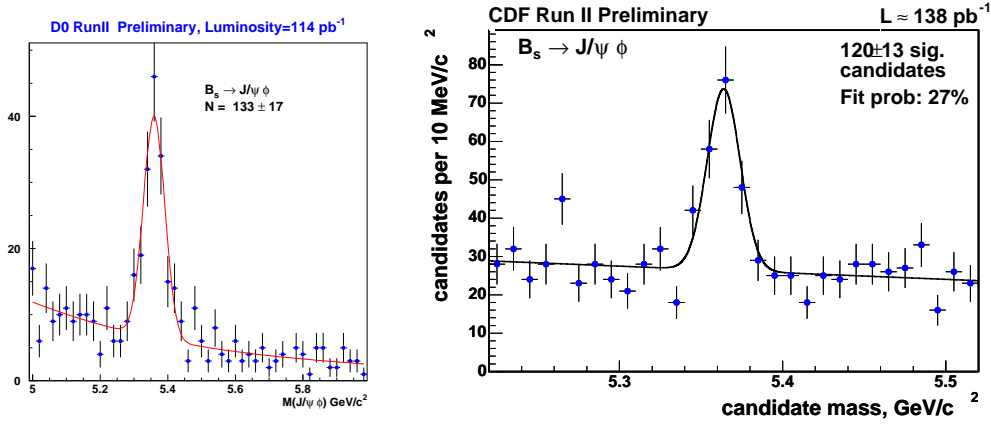


Figure 7: Measured $J/\psi\phi$ invariant mass distribution of B_s meson candidates compared to the result of an unbinned log likelihood fit for D0 (left) and CDF (right).

are used to check the fit technique and to estimate systematics.

The measured invariant mass of the B_s meson candidates of CDF and D0 is compared with the fit results in Figure 7. With over 120 candidates each, these are the largest samples of fully reconstructed B_s mesons in the world. The D0 result for the B_s meson mass is $5360 \pm 5 \text{ MeV}/c^2$ with 114 pb^{-1} . The CDF result is $5365.5 \pm 1.3(\text{stat}) \pm 0.9(\text{sys}) \text{ MeV}/c^2$ with 138 pb^{-1} , which is the best measurement in the world and is significantly better than the world average of $5369.6 \pm 2.4 \text{ MeV}/c^2$.

To measure the lifetime, τ , of the B_s meson, we need two further pieces of information: the p_T of the B_s meson, which is well-measured since this is a fully reconstructed decay; and the 2D decay length, L_{xy} , which is the distance from the secondary vertex formed by the B_s meson daughters to the primary interaction

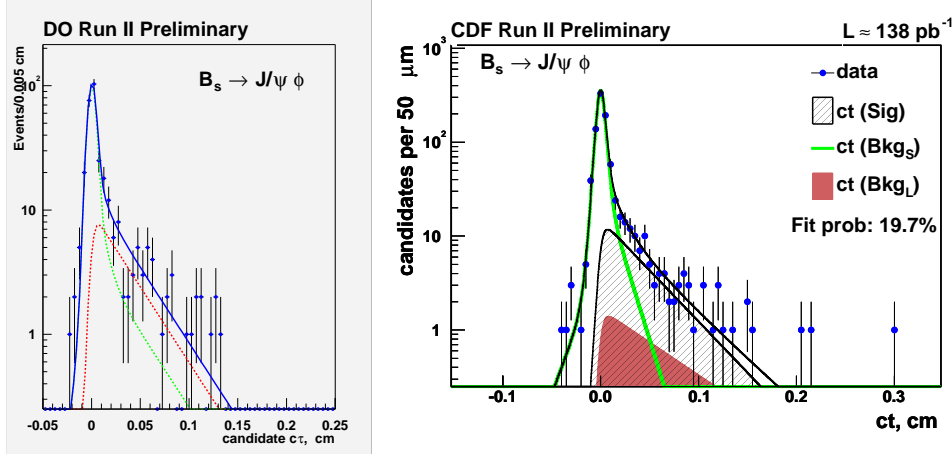


Figure 8: The proper decay length of D0 (left) and CDF (right) B_s meson candidates compared to the result of an unbinned log likelihood fit.

point. The measured proper decay length, $c\tau = L_{xy} \frac{m_B^B}{p_T^B}$, of the B_s meson candidates is compared to the result of an unbinned log likelihood fit with a signal component and a short-lived and long-lived background component in Figure 8. The CDF result is $1.33 \pm 0.14(stat) \pm 0.02(sys)$ ps with 138 pb^{-1} . The D0 result is $1.19 \pm_{0.16}^{0.19} (stat) \pm 0.14(sys)$ ps with 114 pb^{-1} . These measurements are much less precise than the world average value of 1.461 ± 0.057 ps. Alternatively, semi-leptonic decays provide larger signal yields but suffer from uncertainty in the B_s meson p_T due to the unreconstructed neutrino. With large data samples, the semileptonic modes will become systematics limited due to this partial reconstruction, while the statistics limited fully reconstructed modes will continue to improve in sensitivity. In future, the fully reconstructed modes will be used to search for CP violation in the B_s system.

3.4 Mass and Lifetime of the Λ_b baryon

These Λ_b baryon analysis also use the di-muon trigger to collect the decay mode $\Lambda_b \rightarrow J/\psi \Lambda$. The neutral Λ is long-lived and travels about 10 cm on average before decaying into a proton and pion - there are typically no hits in the inner silicon layers for these tracks - with the proton carrying off most of the momentum. The topologically similar $B^0 \rightarrow J/\psi K_s^0$ final state is used to check the fit technique and to estimate systematics.

The CDF result for the Λ_b baryon mass is $5620.4 \pm 1.6(stat) \pm 1.2(sys)$ MeV/ c^2

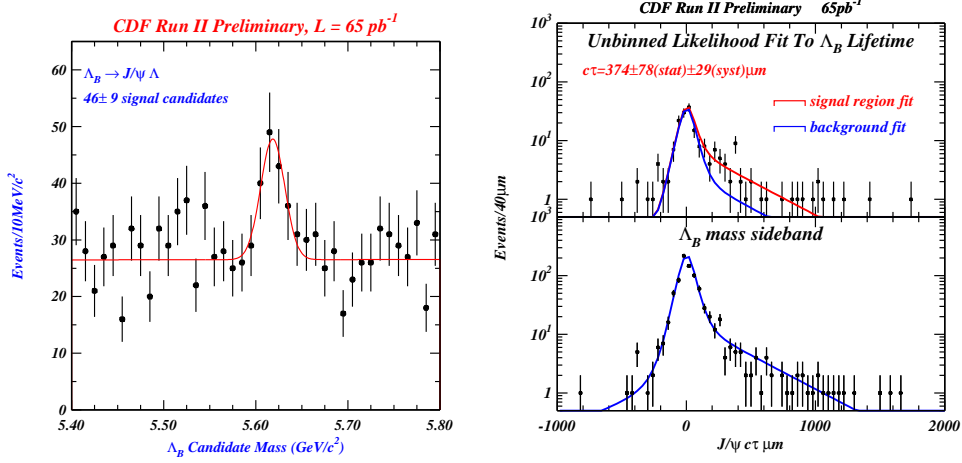


Figure 9: CDF $\Lambda_b \rightarrow J/\psi\Lambda$ candidates: invariant mass distribution (left) and proper decay length (right) in the peak region (top) and the sideband region (bottom).

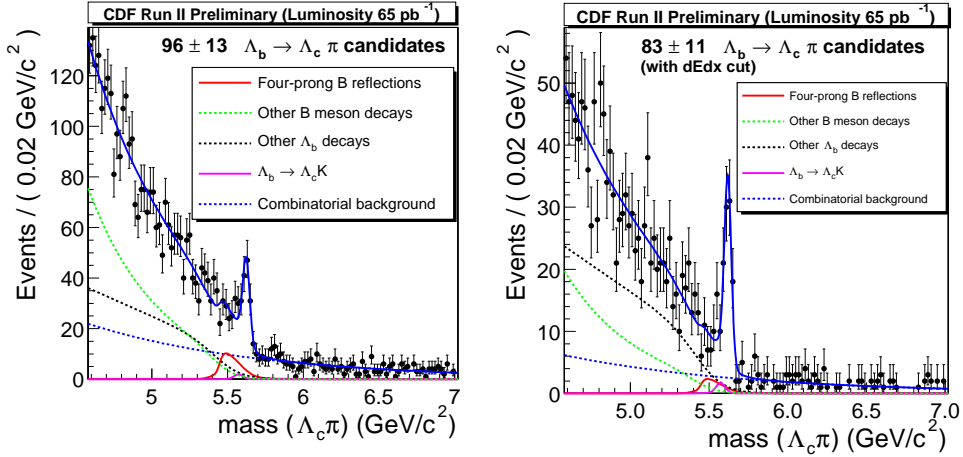


Figure 10: CDF $\Lambda_b \rightarrow \Lambda_c\pi$ with $\Lambda_c \rightarrow pK\pi$ candidates before (left) and after (right) using dE/dx particle identification information.

with 65 pb^{-1} , which is already much better than the world average of $5624 \pm 9 \text{ MeV}/c^2$. This decay mode allows the first measurement of the Λ_b lifetime from a fully reconstructed decay. The measured proper decay length of the CDF $J/\psi\Lambda$ candidates is compared with the fit result in Figure 9. The CDF result is $1.25 \pm 0.26(\text{stat}) \pm 0.10(\text{sys}) \text{ ps}$ with 65 pb^{-1} and the D0 result is $1.05 \pm_{0.18}^{0.21}(\text{stat}) \pm 0.12(\text{sys}) \text{ ps}$ with 114 pb^{-1} . Other decay modes like $\Lambda_b \rightarrow \Lambda_c\pi$ with $\Lambda_c \rightarrow pK\pi$ really need particle identification to reduce background, as illustrated by Figure 10.

Decay mode	Yield
$B^0 \rightarrow K\pi$	148 ± 17
$B^0 \rightarrow \pi\pi$	39 ± 14
$B_s \rightarrow KK$	90 ± 17
$B_s \rightarrow K\pi$	3 ± 11

Table 3: The CDF yield of B meson candidates in two-body charmless B decays in 65 pb^{-1} . The error is statistical only.

The current world average value for the Λ_b lifetime is $1.229 \pm 0.080 \text{ ps}$, which is a bit below the predicted range from Heavy Quark Expansion theory, as shown in Figure 11. This has caused quite a bit of theoretical activity. It will be interesting to see if this difference persists with higher statistics in fully reconstructed decay modes.

3.5 Two-Body Charmless B decays

With the displaced two-track trigger, CDF has observed two-body charmless B decays, with about 300 candidates in 65 pb^{-1} . The broad width of the invariant mass distribution, assuming the pion mass, for the $B^0 \rightarrow h^\pm h^\mp$ signal shown in Figure 12, is due to the four decay channels $B_d \rightarrow \pi\pi$, $B_d \rightarrow K\pi$, $B_s \rightarrow K\pi$ and $B_s \rightarrow KK$. The goal is to measure the four relative fractions and to separate $B_d^0 \rightarrow K^+\pi^-$ from $\bar{B}_d^0 \rightarrow K^-\pi^+$ in order to measure the direct CP asymmetry. Given the limited particle identification capabilities provided by the invariant mass resolution and dE/dx , it is only possible to disentangle the various contributions in a statistical way. The invariant mass versus $\alpha = q_1 \times (1 - \frac{p_1}{p_2})$, where p_1 and q_1 are the momentum and charge of the lower momentum track, allow separation of particles from antiparticles. The yield for $B_s \rightarrow KK$ is measured to be $90 \pm 17(\text{stat}) \pm 17(\text{sys})$ events, a first observation of this decay mode. The fit results for the yield of all four B decay modes are summarized in Table 3. The measured ratio of branching ratios $\frac{BR(B_d^0 \rightarrow \pi\pi)}{BR(B_d^0 \rightarrow K\pi)} = 0.26 \pm 0.11(\text{stat}) \pm 0.05(\text{sys})$ is found to agree well with the world average of 0.25 ± 0.06 .

The measured direct CP asymmetry with 65 pb^{-1} is:

$$A_{CP} = \frac{\bar{B}_d^0 \rightarrow K^-\pi^+ - B_d^0 \rightarrow K^+\pi^-}{\bar{B}_d^0 \rightarrow K^-\pi^+ + B_d^0 \rightarrow K^+\pi^-} = 0.02 \pm 0.15(\text{stat}) \pm 0.017(\text{sys})$$

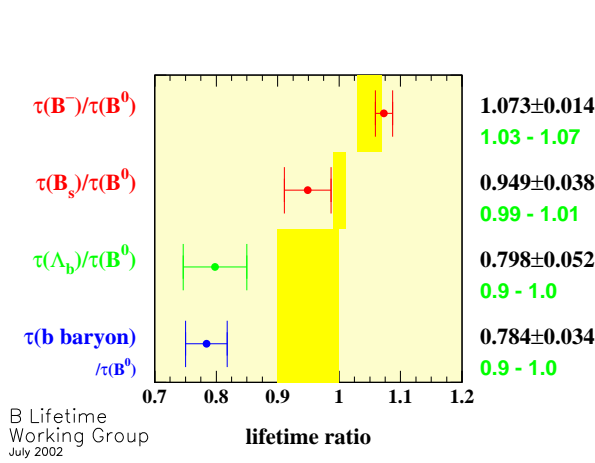


Figure 11: World average B hadron lifetimes (points) compared to range predicted by Heavy Quark Expansion theory (yellow band).

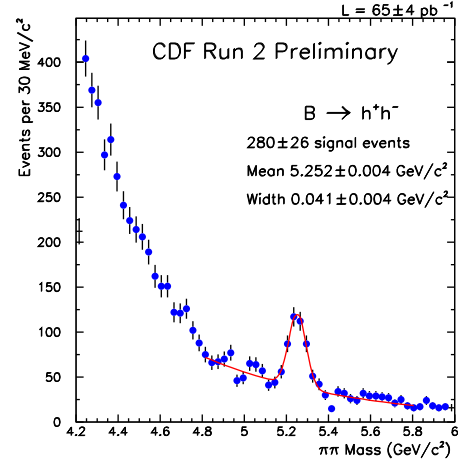


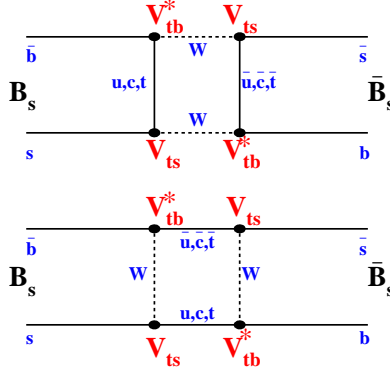
Figure 12: The invariant mass distribution of two-body charmless B decay candidates, where the pion mass is assumed, in 65 pb^{-1} of CDF data.

The recent result from BABAR¹⁶ is $A_{CP} = -0.102 \pm 0.050 \pm 0.016$. With a factor of 3 times more data already in hand for CDF along with improved detector and trigger performance and reconstruction, the statistical error from CDF can be expected to decrease significantly in the near future.

3.6 Prospects for Measurement of the B_s Mixing Frequency

Particle-antiparticle mixing occurs since the weak interaction eigenstates are linear combinations of the mass eigenstates. The box diagrams shown in Figure 13 allow a B_s^0 meson to oscillate into a \bar{B}_s^0 with a frequency proportional to the CKM matrix element V_{ts} . The ratio of the $B^0\bar{B}^0$ and $B_s^0\bar{B}_s^0$ mixing frequencies is then proportional to the length of one of the sides of the unitarity triangle. Therefore, a measurement of the B_s mixing frequency is very interesting as a test of the Standard Model. In addition, some models beyond the Standard Model predict very large mixing frequencies. There are four ingredients to a B_s mixing analysis:

- **Initial flavor of the B_s meson at production.** One technique to determine if the meson is produced as B_s^0 or \bar{B}_s^0 is to use the charge of the closest fragmentation track to the B_s meson candidate. A useful figure of merit is ϵD^2 , where ϵ is the efficiency of the tagging technique and the dilution D is the net fraction of correct tags. Hadron collider experiments have 5% for


 Figure 13: Box diagrams for the $B_s^0 \rightarrow \bar{B}_s^0$ transition.

- ϵD^2 , whereas BABAR and BELLE typically have values of 27%. For example, an experiment with 1000 B_s meson candidates with a ϵD^2 of 5% is equivalent to a sample of 50 events where the tag is known absolutely.
- Final flavor of the B_s meson at decay.** For fully hadronic $B_s^0 \rightarrow D_s^- \pi^+$ and semileptonic $B_s^0 \rightarrow D_s^- \ell^+ \nu_\ell$, both with $D_s^- \rightarrow \phi \pi^-$, the flavor of the B_s meson is given by the charge of the decay products. Obviously, charge symmetric final states like $B_s^0 \rightarrow J/\psi \phi$ are useless to mixing analysis.
 - Proper decay time.** The B_s meson mixing frequency is so fast that it has not yet been resolved by any experiment. The world average 95% confidence level limit is $\Delta m_s \geq 14.4 \text{ ps}^{-1}$, which means that the B_s mesons oscillate very fast compared to the B_s lifetime of 1.5 ps! This makes time-integrated measurements insensitive and so the mixing probability must be measured as a function of the proper decay time. If the true mixing frequency is close to this limit, both the semileptonic and fully reconstructed samples will contribute to the measurement. However, if the mixing frequency is above 20 ps^{-1} , the semileptonic sample loses sensitivity due to the poorer proper time resolution from the uncertainty on the p_T of the partially reconstructed B_s meson. The fully reconstructed sample has lower statistics but better proper time resolution.
 - Large samples of B_s mesons** are required to combat the dilution of statistical power from the initial flavor tagging and to resolve the oscillation frequency as a function of proper decay time - a good rule of thumb is 1000 events.

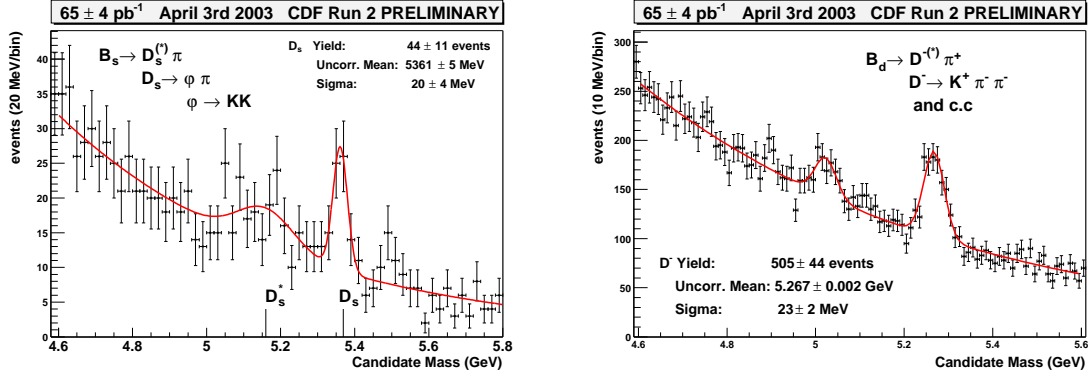


Figure 14: Fully reconstructed B_s (left) and B^0 (right) decays collected with the CDF displaced two track trigger.

CDF observes about 50 candidates in 65 pb^{-1} for the golden fully reconstructed decay mode, $B_s^0 \rightarrow D_s^- \pi^+$, with $D_s^- \rightarrow \phi \pi^-$ and $\phi \rightarrow K^+ K^-$. Note that improvements in the silicon coverage and trigger logic will increase the event yield per pb^{-1} , as will reconstruction of additional decay modes. The measured invariant mass distributions for the B_s and the $B^0 \rightarrow D^- \pi^+$ candidates, which have similar final state kinematics, are shown in Figure 14. Particle identification will improve the sample purity and improvements to the tracking algorithms will sharpen the invariant mass resolution. CDF measures the ratio of branching ratios:

$$\frac{f_s BR(B_s \rightarrow D_s^- \pi^+)}{f_d BR(B^0 \rightarrow D^- \pi^+)} = 0.41 \pm 0.11(stat) \pm 0.11(BR) \pm 0.07(sys)$$

4 Electroweak Physics

There is a huge amount of interesting physics associated with events containing W and Z bosons, everything from the precise measurements of fundamental properties like the W boson mass and diboson couplings, to top physics and searching for associated Higgs production. The leptonic decays, $W \rightarrow \ell \nu$ and $Z \rightarrow \ell^+ \ell^-$, where ℓ is an electron or muon, leave a clean signature in the detectors that can be triggered on with high efficiency (90-98%) and low background. Final states containing τ leptons are of interest to many searches for new physics, so the experiments have also designed τ triggers in Run II.

Rather like Type 1A Supernovae,¹⁷ W and Z bosons are our standard candles for understanding what we see in our detectors. Z decays to $e^+ e^-$ and $\mu^+ \mu^-$

give high purity samples from which to measure electron and muon identification efficiencies. The well-known Z boson mass provides an energy and momentum scale calibration point for high p_T physics, much like the J/ψ does at lower p_T . Z decays to $b\bar{b}$ also provide an important calibration sample for studying high p_T b-jets for the top mass measurement and Higgs boson searches.

4.1 W and Z Boson Production Cross-Section

W boson candidates are events with a high p_T lepton and large missing transverse energy (MET). Both experiments require the lepton E_T and the MET to be greater than 25 GeV in the electron channel and to be greater than 20 GeV in the cleaner muon channel. The current CDF result only uses central electrons with $|\eta| < 1.0$ and central muons with $|\eta| < 0.6$. Future results will use the increased acceptance from the Run II upgrades. The current D0 result also only uses central electrons with $|\eta| < 1.1$ but the D0 muon acceptance extends much further to $|\eta| < 1.6$.

Z boson candidates are events with two oppositely charged high p_T leptons. Both experiments require the lepton to have E_T greater than 25 GeV and to be in the central region for the electron channel. CDF requires the muon p_T to be greater than 20 GeV/c² and $|\eta| < 0.6$, while D0 requires the muon p_T to be greater than 15 GeV/c² and $|\eta| < 1.8$.

The production cross-section is simply the number of events passing the selection cuts in the data minus the expected background, all divided by the integrated luminosity and the signal acceptance after all selection cuts. Most of the backgrounds are estimated from MC simulation, but the background from QCD jets that somehow fake leptons is estimated directly from the data. The acceptance, or efficiency for the signal events, is estimated from MC simulation, using lepton identification efficiencies measured with Z data. The event yields and measured cross-section times branching ratio are summarized in Table 4. The results are all in good agreement with the NNLO theory prediction¹⁸ of 2.731 ± 0.0002 nb for $W \rightarrow \ell\nu$ and 0.252 ± 0.009 nb for $Z \rightarrow \ell^+\ell^-$.

Although not directly used in these measurements, the W transverse mass distribution, $M_T = \sqrt{2E_\ell E_\nu(1 - \cos\phi_{\ell\nu})}$, will be crucial to the measurement of the W boson mass at the Tevatron. The measured W transverse mass distribution is compared to the total expectation from Monte Carlo simulation of the signal and backgrounds for CDF $W \rightarrow e\nu$ candidates and for D0 $W \rightarrow \mu\nu$ candidates

	CDF: all 72 pb^{-1}		D0: e 42 pb^{-1} , μ 17 pb^{-1}	
Channel	Events	$\sigma(W) \times BR(W \rightarrow \ell\nu)$ (nb)	Events	$\sigma(W) \times BR(W \rightarrow \ell\nu)$ (nb)
e	38625	$2.64 \pm 0.01 \pm 0.09 \pm 0.16$	27370	$2.84 \pm 0.02 \pm 0.13 \pm 0.28$
μ	21599	$2.64 \pm 0.02 \pm 0.12 \pm 0.16$	7352	$3.23 \pm 0.13 \pm 0.10 \pm 0.32$
τ	2346	$2.62 \pm 0.07 \pm 0.21 \pm 0.16$	-	-

	CDF: all 72 pb^{-1}		D0: e 42 pb^{-1} , μ 32 pb^{-1}	
Channel	Events	$\sigma(Z) \times BR(Z \rightarrow \ell\ell)$ (nb)	Events	$\sigma(Z) \times BR(Z \rightarrow \ell\ell)$ (nb)
e	1830	$0.267 \pm 0.006 \pm 0.015 \pm 0.016$	1139	$0.275 \pm 0.009 \pm 0.009 \pm 0.028$
μ	1631	$0.246 \pm 0.006 \pm 0.012 \pm 0.015$	1585	$0.264 \pm 0.007 \pm 0.017 \pm 0.026$

Table 4: Measured event yields and cross-sections times branching ratios for $W \rightarrow \ell\nu$ and $Z \rightarrow \ell\ell$ events. The errors are ordered as statistical, systematic and luminosity.

in Figure 15. Further advances in alignment and tracking algorithms, simulation of passive detector material and the calorimeter will sharpen these distributions and improve the agreement.

4.2 W Width

The measured W and Z cross-section times branching ratios are already systematics limited. However, most of the systematics cancel in the ratio, from which the W boson width can be indirectly measured:

$$R = \frac{\sigma(p\bar{p} \rightarrow W)}{\sigma(p\bar{p} \rightarrow Z)} \frac{\Gamma(Z)}{\Gamma(Z \rightarrow \ell\ell)} \frac{\Gamma(W \rightarrow \ell\nu)}{\Gamma(W)}$$

The ratio of the total W and Z production cross-sections and the W leptonic decay width are well-predicted by theory and the branching ratio of Z to leptons is well-measured by the LEP experiments. The indirect measurement of the W width is 2.181 ± 0.074 GeV. The world average, which is dominated by results from CDF and D0 from Run I, is 2.118 ± 0.042 GeV.

4.3 Forward-Backward Asymmetry

The Tevatron has a unique high mass reach for the forward-backward asymmetry of e^+e^- pairs:

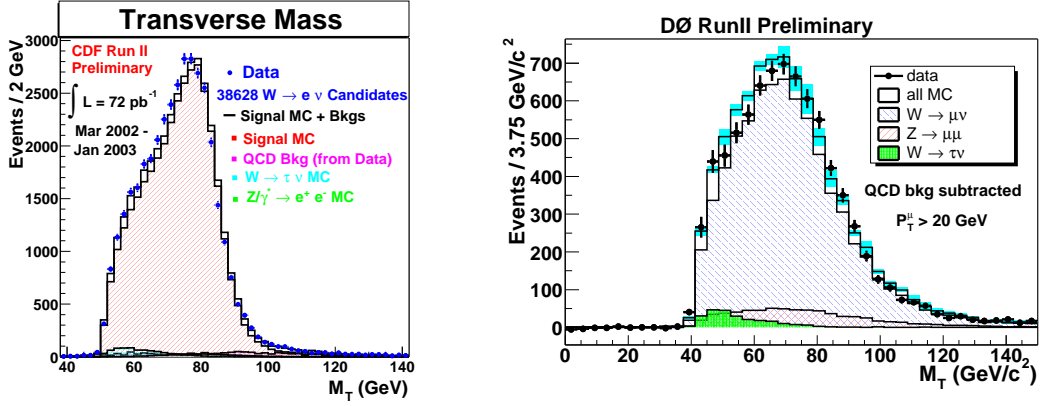


Figure 15: Measured W transverse mass distribution for $W \rightarrow e\nu$ candidates in CDF (left) and $W \rightarrow \mu\nu$ candidates in D0. D0 has already subtracted the background from QCD fake leptons.

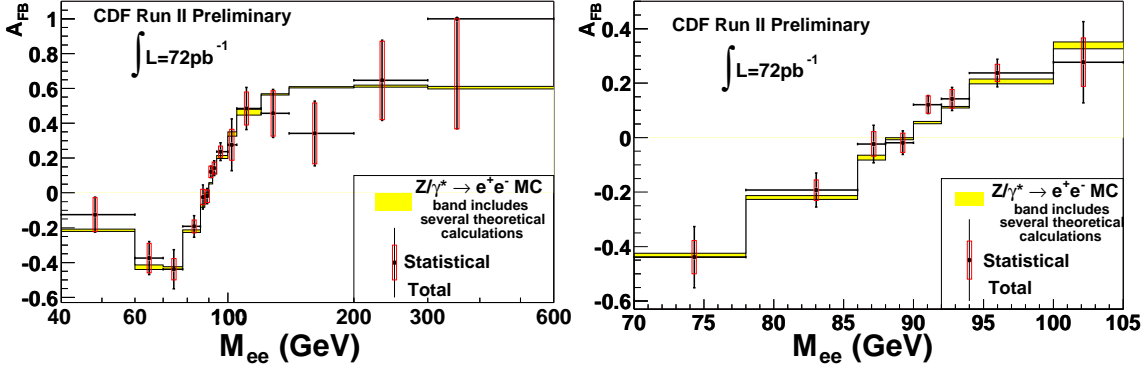


Figure 16: The measured asymmetry of e^+e^- pairs in 72 pb^{-1} of CDF data (left) with a zoom into the high statistics Z pole region (right). The band indicates the range of several theoretical predictions.

$$A_{FB} = \frac{d\sigma(\cos\theta > 0) - d\sigma(\cos\theta < 0)}{d\sigma(\cos\theta > 0) + d\sigma(\cos\theta < 0)}$$

The increased acceptance from the new CDF forward calorimeter allows electron identification out to $|\eta| < 3$. The measured asymmetry versus the e^+e^- invariant mass from CDF is compared to prediction from theory in Figure 16. This measurement probes the $Z-\gamma$ interference and complements the direct search for Z' bosons.

5 Top Physics

All the Run I measurements of top quark properties were based on a sample of about 30 events in each experiment. With 2000 pb^{-1} of data, both experiments should have over 1000 events and detailed studies of top quark properties will become possible for the first time. Several models beyond the Standard Model predict modifications to top quark properties and allow decays to more exotic particles, so the top quark is an interesting object to examine for signs of new physics.^{20,21}

5.1 Top Pair Production Cross-Section

The dominant Standard Model production mechanism of top quarks at the Tevatron is pair production via the strong interaction, with 85% from $q\bar{q}$ annihilation and 15% from gluon fusion at $\sqrt{s} = 1.96$ TeV. The predicted cross-section from NLO theory²² is in the range 5.8-7.4 pb for $m_t = 175$ GeV/ c^2 . Note that an increase of 5 GeV/ c^2 in the assumed top quark mass causes the predicted cross-section to decrease by about 1 pb and vice versa. The measured top quark mass and production cross-section together test the QCD prediction for the cross-section.

One consequence of the large top quark mass is that with $\Gamma(t \rightarrow Wb) \approx 1.5$ GeV, the top quark decays very fast in 10^{-25} s to a W boson and a b quark with a branching ratio of almost 100% in the Standard Model. This is too fast for hadronization, so there are no top mesons or baryons. Therefore, the top quark spin should be directly observable in the angular distribution of the top decay products. The final state is characterised by the W boson decay modes:

- **Dilepton:** $t\bar{t} \rightarrow \ell\nu\ell\bar{\nu}b\bar{b}$ where both W bosons decay leptonically. The experimental signature is 2 isolated oppositely charged high p_T leptons, high MET from the neutrinos and 2 or more jets. The branching ratio is small at 9/81, but this is compensated by the high purity that can be obtained for final states with electrons or muons.
- **Lepton+Jets:** $t\bar{t} \rightarrow \ell\nu q\bar{q}b\bar{b}$ where one W boson decays to leptons and the other decays to quarks. The experimental signature is 1 isolated high p_T lepton, high MET from the neutrino and, in principle, 4 or more jets. The branching ratio is higher at 36/81, but the backgrounds from W +jet pro-

Experiment (Luminosity)	Technique	$\sigma(t\bar{t})$ (pb)
<i>Dilepton</i>		
CDF (72 pb^{-1})	2 leptons	$13.2 \pm 5.9 \pm 1.5 \pm 0.8$
CDF (126 pb^{-1})	lepton+track	$7.3 \pm 3.4 \pm 1.7 \pm 0.4$
D0 (98 pb^{-1})	2 leptons	$8.7 \pm_{4.7}^{6.4} \pm_{2.0}^{2.7} \pm 0.9$
<i>Lepton+Jets</i>		
CDF (108 pb^{-1})	SVX b-tag	$4.5 \pm 1.4 \pm 0.7 \pm 0.3$
D0 (45 pb^{-1})	SVX b-tag	$10.8 \pm_{4.0}^{4.9} \pm_{2.0}^{2.1} \pm 1.1$
D0 (45 pb^{-1})	CSIP b-tag	$7.9 \pm_{3.6}^{4.4} \pm_{1.8}^{2.1} \pm 0.7$
D0 (90 pb^{-1})	SMT+KIN	$8.0 \pm_{2.1}^{2.4} \pm_{1.5}^{1.7} \pm 0.8$

Table 5: Measurements of the top pair production cross-section from CDF and D0 in Run II. The errors are ordered as statistical, systematic and luminosity. Lepton means electron or muon here.

duction are large, so typically one jet is required to be tagged as likely to contain a b quark (b-tag) to improve the signal purity of the sample.

- **All-hadronic:** $t\bar{t} \rightarrow q\bar{q}q\bar{q}b\bar{b}$ where both W bosons decay to quarks. The experimental signature is 6 or more jets. The branching ratio is 36/81 but this channel is swamped by huge backgrounds from QCD multi-jet production. Typically two b-tags are required to suppress this background.

Top pair production was observed in all of these final states in Run I. The combined cross-section results from Run 1 are 5.7 ± 1.6 pb from D0,²³ assuming the central value of $m_t = 172.1$ GeV/ c^2 from the D0 top mass measurement, and $6.5 \pm_{1.4}^{1.7}$ pb from CDF,²⁴ assuming the central value of $m_t = 175$ GeV/ c^2 from the CDF top mass measurement.

All of the Run II top pair production cross-section measurements so far, summarized in Table 5, are from counting experiments: the cross-section, $\sigma(t\bar{t})$, is the number of events passing the selection cuts in the data minus the expected background, all divided by the integrated luminosity and the signal acceptance after all selection cuts. The difficult part, of course, is the background estimate.

In the dilepton channel, the main physics backgrounds from WW and $Z \rightarrow \tau^+\tau^-$ are estimated from MC simulation. Instrumental backgrounds from QCD and W+jets events, where a jet fakes a lepton, are estimated from a parameterisa-

Source	ee	$\mu\mu$	$e\mu$	Total
Background	0.10 ± 0.06	0.09 ± 0.04	0.10 ± 0.04	0.30 ± 0.12
$t\bar{t} \rightarrow \ell\nu\ell\bar{\nu}b\bar{b}$	0.47 ± 0.05	0.59 ± 0.07	1.44 ± 0.16	2.50 ± 0.30
SM expectation	0.57 ± 0.08	0.68 ± 0.09	1.54 ± 0.17	2.80 ± 0.32
Data	1	1	3	5

Table 6: CDF dilepton channel event yields compared with expectation from background and signal processes for about 72 pb^{-1} . The $t\bar{t}$ cross-section is assumed to be 6.7 pb.

Source	ee	$\mu\mu$	$e\mu$	Total
Background	0.58 ± 0.51	0.70 ± 0.44	0.60 ± 0.42	1.88 ± 0.79
$t\bar{t} \rightarrow \ell\nu\ell\bar{\nu}b\bar{b}$	0.63 ± 0.10	0.46 ± 0.10	1.73 ± 0.26	2.81 ± 0.30
SM expectation	1.21 ± 0.52	1.16 ± 0.45	2.33 ± 0.49	4.69 ± 0.64
Data	2	0	3	5

Table 7: D0 dilepton channel event yields compared with expectation from background and signal processes for about 98 pb^{-1} . The $t\bar{t}$ cross-section is assumed to be 7 pb.

tion developed and tested on large samples of jet data. For ee and $\mu\mu$ final states, Drell-Yan processes also contribute, with fake MET due to mismeasurement of jets or leptons. Most of this background will have a dilepton invariant mass close to the Z boson mass and can be rejected with specific cuts. The observed number of events in data is compared to the expectation for $t\bar{t}$ signal and background for CDF in Table 6 and for D0 in Table 7. CDF has also performed an analysis where the second lepton candidate is simply an isolated, prompt track without any lepton identification criteria. This increases the acceptance for $t\bar{t}$ dilepton events by about 50% with respect to an analysis requiring two isolated identified leptons, but at the cost of higher backgrounds levels, with typical S:N being 3:2 rather than 5:1.

In the lepton+jets channel, the dominant background is from W +jets production. The background rate cannot be estimated directly from MC since the uncertainty of about 30% from the Leading-Order cross-section would destroy the significance of the $t\bar{t}$ signal. More accurate NLO calculations of $W + \geq 3$ jet

	Kinematic		Soft Muon Tag	
Source	e +jets	μ +jets	e +jets	μ +jets
Background	6.8 ± 1.6	11.7 ± 1.9	1.12 ± 0.92	2.18 ± 0.96
$t\bar{t} \rightarrow \ell\nu\ell\bar{\nu}b\bar{b}$	5.3	6.8	2.9	4.5
SM expectation	12.1 ± 1.6	18.5 ± 1.9	4.02 ± 0.92	6.68 ± 0.96
Data	12	14	7	8

Table 8: D0 lepton+jets channel orthogonal kinematic and soft muon tag (KIN+SMT) analysis event yields compared with expectation from background and signal processes for about 90 pb^{-1} . The $t\bar{t}$ cross-section is assumed to be 7 pb.

processes are very complex and will not be completed for several years.

One approach used by D0 is to improve the sample purity by applying kinematic and topological cuts that take advantage of the higher total transverse energy and larger aplanarity of $t\bar{t}$ events compared to background events. An orthogonal approach with higher purity is to apply looser kinematic and topological cuts and look in addition for a soft muon from a semileptonic b decay (such events are vetoed from the preceding kinematic analysis). However, the semileptonic branching ratio is only 10% so even with 2 b jets per $t\bar{t}$ event, only 19% of $t\bar{t}$ events contain a muon from semileptonic b decays. In both approaches, the W +jet background rate is estimated directly from the data by extrapolation from the lower jet multiplicity regions to the signal ≥ 4 jet region. The background from QCD multijet events is also estimated directly from the data. The observed number of events is compared to the expectation from $t\bar{t}$ signal and background in Table 8.

An alternative approach with higher purity and efficiency is to look for displaced tracks from the decay of the long-lived b hadrons. D0 can use these techniques for the first time in Run II with the new axial magnetic field and silicon subdetectors. One method developed by CDF in Run I relies on the direct reconstruction of significantly displaced secondary vertices (SVX). Another method is to require a certain number of significantly displaced tracks per jet (CSIP). To give you an idea of the efficiency and rejection power of these techniques, the expected efficiency of the CDF SVX method to tag at least one b -jet in a $t\bar{t}$ MC event is about 55%, while only about 3% of $t\bar{t}$ MC events have at least one c -jet tagged and only about 1% of $t\bar{t}$ MC events have at least one light flavor ($u\bar{d}s\bar{g}$)

jet mis-tagged. Given the ongoing improvement of tracking alignment and algorithms, these efficiencies can be expected to improve in future. After requiring at least one jet to be b -tagged, the backgrounds can be grouped into four categories:

- **W +jet production where the b -tag algorithm correctly tags a jet containing heavy flavor.** The basic assumption used to estimate this background is that the fraction of W +jets events containing heavy flavor (b and c quarks from $Wb\bar{b}$, $Wc\bar{c}$ and Wc) is well predicted by the MC simulation. Therefore, this technique does not depend on the absolute rate from the MC model. The background rate from W +jet processes with heavy flavor can be estimated by multiplying the number of pre-tag observed W +jets events by the heavy flavor fraction times the efficiency of the b -tag algorithm for W +jet processes with heavy flavor. Since the expected pre-tag background from QCD multi-jet production is a significant (10%) fraction of the number of pre-tag W +jet events, this background is first subtracted. Since $t\bar{t}$ events form a significant fraction of the number of pre-tag W +jet events in the signal region, this background estimate is iterated several times using the measured number of $t\bar{t}$ events.
- **W +jet production where the b -tag algorithm mistags a light flavor jet.** A mistag rate is parameterized in a large sample of jet data as a function of several variables including jet E_T , $|\eta|$ and number of tracks per jet. The background level is estimated by applying this mistag matrix to the pre-tag W +jet data.
- **QCD multi-jet production, where a jet fakes a lepton.** This background may contain significant amounts of heavy flavor, so a tag rate is measured in a complementary QCD-dominated data sample that has the same lepton and jet requirements as the signal region but low MET. The background level is estimated by applying this tag rate matrix to the pre-tag W +jet data times the pre-tag QCD background fraction.
- **Other backgrounds from WW , WZ , ZZ , $Z \rightarrow \tau^+\tau^-$ and single top production.** These can be estimated directly from MC simulation.

The estimated backgrounds from these different sources are compared to the number of events observed in the data as a function of jet multiplicity for the CDF SVX and D0 CSIP b -tag methods in Figure 17. The good agreement in the

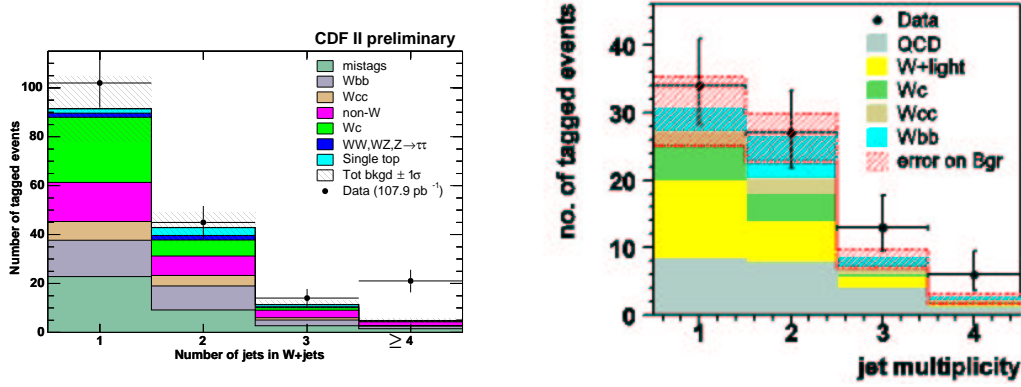


Figure 17: The observed event yield and expectation from background for the CDF SVX method (left) and the D0 CSIP method (right) as a function of jet multiplicity.

background dominated 1- and 2-jet region gives confidence in the reliability of the background estimates. The excess in the 3 and ≥ 4 jet regions is attributed to $t\bar{t}$ production.

5.2 Top Mass

Good agreement between the direct measurements of the top quark mass and the W boson mass (green ellipse) and the indirect prediction from the interpretation of other precision electroweak measurements (red ellipse) is seen in Figure 18. Both prefer a lighter value for the Standard Model Higgs boson mass. The χ^2 of the global Standard Model fit to all precision electroweak measurements²⁵ with respect to the minimum value is shown as a function of the Higgs boson mass in Figure 18. At 95% confidence level, the Higgs boson mass is less than 211 GeV/c². However, the top and Higgs masses are strongly correlated in the global Standard Model fit - a 5 GeV/c² shift (one standard deviation) in the top quark mass produces a 35% shift in the central predicted value for the Higgs boson mass.²⁶ Clearly, a more accurate and precise measurement of the top quark mass is crucial to sharpening the constraint on the Higgs boson mass.

CDF has measured the top quark mass in the lepton+jets channel for events with 4 or more jets and at least one SVX b -tag. Twenty-two candidates are observed in 108 pb^{-1} of Run II data, with a background expectation of 6.5 ± 2.0 . As in Run I, a single variable, the event-by-event reconstructed top mass, is chosen as the best estimator for the true top quark mass. For each event, there are

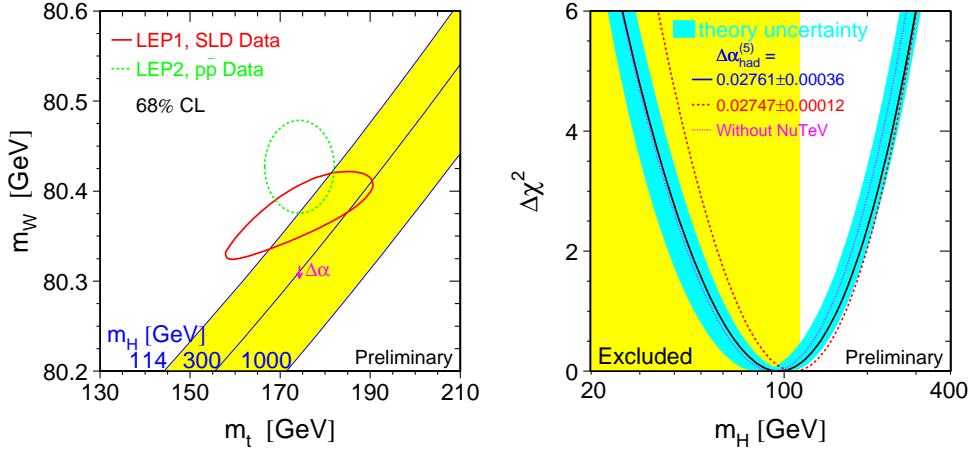


Figure 18: Comparison²⁵ of direct measurements of the W boson mass and the top quark mass with the indirect predictions from the Standard Model (left). The $\Delta\chi^2$ of the global fit to all precision electroweak data as a function of the Standard Model Higgs boson mass (right).

12 possible jet-parton combinations with two solutions each for the neutrino p_z . The b -tag information reduces the number of combinations to 12. A constrained kinematic fit is used to choose the best combination (lowest χ^2) and to improve the raw invariant mass resolution. A Gaussian constraint with width Γ_W and mean as the world average W boson mass is applied to the $l\nu$ and jj reconstructed W masses. A Gaussian constraint with width Γ_t and mean as the fitted top mass is applied to the lvb and jjb reconstructed top masses. The lepton and jet energies are allowed to vary within experimental errors as are the transverse momentum components of the underlying event. The reconstructed top mass is compared to the result of an unbinned log likelihood fit in Figure 19, where the signal and background shapes are derived from MC simulation. While CDF expects a statistical error of $9 \text{ GeV}/c^2$, the result is $m_t = 177.5 \pm_{9.4}^{12.7}(\text{stat}) \pm 7.1(\text{sys}) \text{ GeV}/c^2$. The systematic error is dominated by the jet energy scale uncertainty, which will soon be reduced with improved modeling of the response of the new forward calorimeter to low energy particles.

D0 has recently updated their Run I measurement of the top quark mass with a more powerful dynamic likelihood technique that gives more weight to better measured events. While D0 expects a statistical error of $5 \text{ GeV}/c^2$, the new

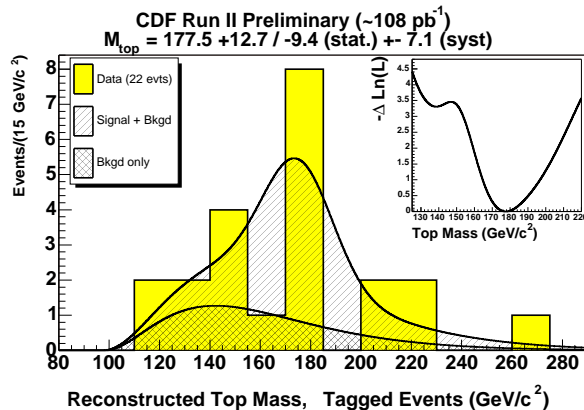


Figure 19: The CDF reconstructed top mass distribution in the lepton+jets channel with 108 pb^{-1} . The inset shows the likelihood as a function of the true top quark mass.

preliminary result is $m_t = 180.1 \pm 3.6 \pm 4.0 \text{ GeV}/c^2$. The statistical error from the old technique was $5.6 \text{ GeV}/c^2$, so the improvement is equivalent to an increase of 2.4 in statistics.

6 QCD

The increase in the Tevatron centre-of-mass energy allows CDF and D0 to observe higher E_T jets than ever before. With such high momentum transfers, jet production is potentially sensitive to a wide variety of new physics. However, the uncertainty in the knowledge of the gluon parton distribution function at high x leads to a significant range for the prediction from Standard Model processes. Independent measurements of the forward-forward and central-forward dijet production cross-section will be essential to constrain the gluon distribution at high- x and separate any signal for new physics.

The good agreement between the measured inclusive jet cross-section from CDF for 85 pb^{-1} and the prediction from NLO QCD over 8 orders of magnitude is shown in Figure 20. The theoretical error at high jet energies is dominated by the uncertainty in the gluon parton distribution function at high x . The uncertainty on the measured inclusive jet cross-section is currently dominated by the jet energy scale systematic, which is expected to be reduced in the near future.

The good agreement between the measured dijet cross-section from D0 with 34 pb^{-1} and the prediction from NLO QCD over 6 orders of magnitude is shown

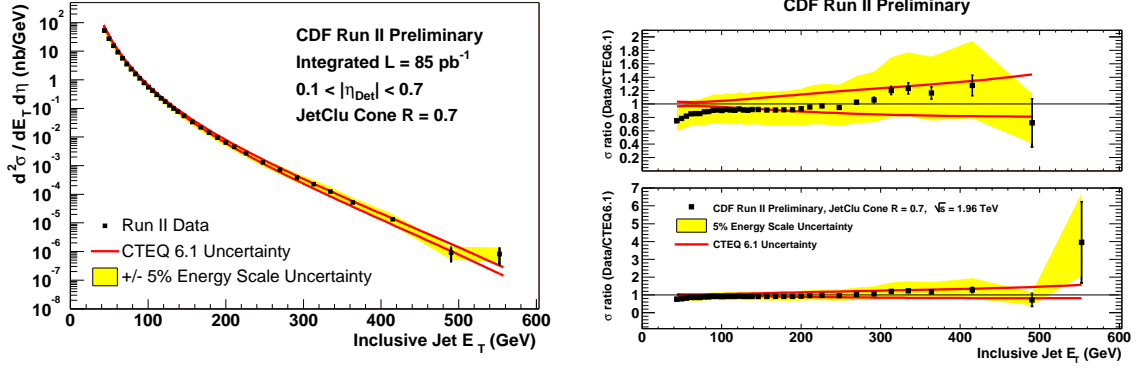


Figure 20: The measured inclusive jet production cross-section from CDF compared to the prediction from NLO QCD.

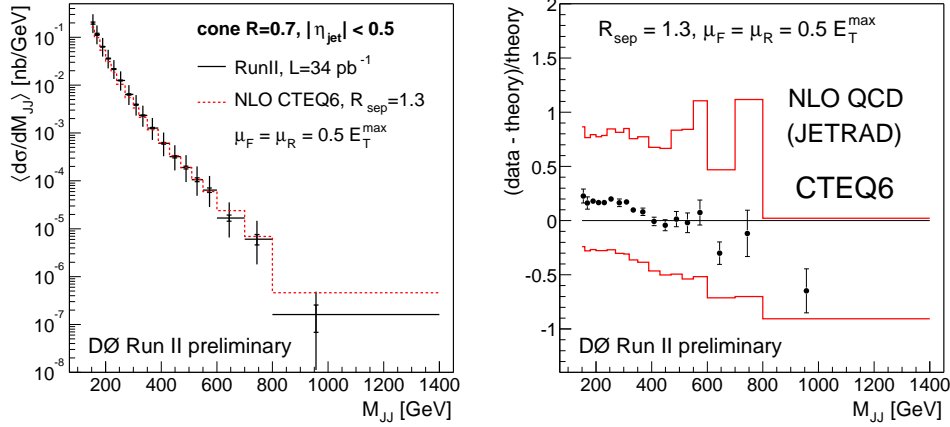


Figure 21: The measured dijet production cross-section from D0 compared to the prediction from NLO QCD.

in Figure 21. As for CDF, the measurement systematics are currently dominated by the jet energy scale systematic.

7 Searches for New Physics

Today, there is nothing new in the Standard Model of particle physics but for the undiscovered mass-giving particle, the Higgs boson. One might conclude that there is nothing much left to do apart from that but more and more precise measurement. However, the Standard Model is incomplete - it does not explain the pattern of masses and mixing angles or the number of quarks and leptons, it cannot unify the strong and electroweak forces, and it does not include gravity.

Direct evidence for physics beyond the Standard Model is provided by the recent observation of neutrino oscillations and the startling finding that dark matter makes up 22% of the energy density in the universe.

Models beyond the Standard Model can unify the strong and electroweak forces and yield candidates for dark matter, and even provide explanations for the hierarchy in the electroweak and gravitational scales. These more general theories make predictions that can be tested at the Tevatron. The Tevatron is the world's highest energy accelerator and can set the most powerful limits with direct searches for new particles. The large range of physics possible at the Tevatron also allows other tests that are sensitive to new physics, like searches for rare decays of the B or D hadrons.

7.1 Extra Dimensions

Extra dimensions solve the hierarchy problem between the electroweak scale (1 TeV) and the Planck scale (10^{19} TeV) by postulating that the Standard Model particles are confined to the usual 4 dimensions but that gravity propagates in extra dimensions.

The Arkani-Hamed, Dimopoulos, Dvali (ADD) model²⁷ predicts n extra dimensions, where the effective 4-dimensional gravitational constant (eg as measured by the Cavendish experiment) can be written as $M_{Pl}^2 = M_S^{n+2} R^n$, where M_S is the fundamental Planck scale and R is the size of the extra dimensions. In order to solve the hierarchy problem and make the electroweak and gravitational scales similar, M_S must be in the few TeV range. The case $n = 1$ implies $R \approx 10^8$ km and is therefore ruled out by the known $1/r^2$ dependence of the gravitational force at large distances. The case $n = 2$ gives $R \approx 1$ mm, and $n = 3$ gives $R \approx 3$ nm. Tabletop gravity experiments and astrophysical constraints impose tight limits on the $n = 2$ case, but are easily eluded for $n \geq 3$. In these theories, the effect of gravity is enhanced at high energies due to the accessibility of numerous excited states of the graviton. Collider experiments can detect extra dimensions in two ways. Virtual graviton exchange will modify fermion or boson pair production. Real graviton emission with a gauge boson or a quark will give monojet or monophoton signatures with large MET since the graviton escapes undetected into the extra dimensions.

D0 has searched for evidence of virtual graviton exchange by looking for an

Channel	95% C.L. on M_S (TeV/c ²)		
	GRW ²⁸	HLZ ²⁹ n=2,3,7	Hewett ³⁰ $\lambda = +1$
D0 di-EM (120 pb^{-1})	1.28	1,42,1.52,1.01	1.14
D0 $\mu\mu$ (100 pb^{-1})	0.88	1.05, 0.88, 0.70	0.79

Table 9: Limits on M_S in the ADD model of extra dimension from dilepton and diphoton channels. Note that M_S depends on the number of extra dimensions only in the HLZ convention.

excess of events at high dilepton or diphoton invariant masses. The experimental signature is 2 electromagnetic clusters with $E_T > 25$ GeV. In the plane of the invariant mass of the dilepton or diphoton pair and the cosine of the scattering angle in the centre-of-mass frame, the observed data is compared in Figure 22 with the expectation from the QCD multi-jet background, other Standard Model processes and the signal from extra dimensions. The data is consistent with no signal and D0 has set the world's best limits of $M_S \geq 1.28$ TeV/c² at 95% C.L. in the GRW²⁸ convention. The limits on M_S are summarised for several different conventions in Table 9 along with the results from the D0 dimuon channel search. With 2000 pb^{-1} , CDF and D0 will be able to probe extra dimensions up to a M_S of 2 TeV/c².

The Randall-Sundrum model³¹ predicts one “small” extra dimension, where the hierarchy is generated by an exponential, called a warp factor, containing the size of the extra dimension. The Randall-Sundrum graviton is a spin-2 boson, with masses and couplings determined by the warp factor, and can be produced on resonances and decay into dilepton pairs.

CDF has looked for resonances in 72 pb^{-1} of dielectron and dimuon data, which is compared to the expectation from Standard Model backgrounds in Figure 23. The data is consistent with no signal and the 95% confidence level contours on the graviton mass are shown in Figure 24.

7.2 Extra Gauge Bosons

Extra Gauge bosons are predicted in many extensions of the Standard Model including Grand Unified Theories, SUSY with R-parity breaking, Little Higgs

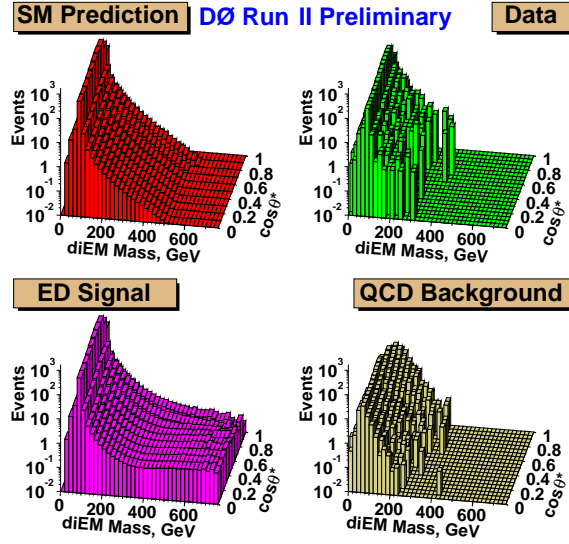


Figure 22: Measured dielectron/diphoton data from 120 pb^{-1} of D0 data compared to expectation from Standard Model processes and signal from extra dimensions.

and Technicolor. Both CDF and D0 have also examined the dilepton data for evidence of resonances at high invariant masses from a Standard Model like extra neutral gauge boson (Z'). No evidence for a signal is found. D0 sets the world's best limit of $m(Z') > 719 \text{ GeV}/c^2$ at 95% C.L. with 100 pb^{-1} . The CDF limit with 72 pb^{-1} is $m(Z') > 665 \text{ GeV}/c^2$ at 95% C.L. With 2000 pb^{-1} , CDF and D0 will be able to discover extra gauge bosons with masses up to $1 \text{ TeV}/c^2$.

7.3 Dijet Resonances

As mentioned in the QCD section, the dijet invariant mass distribution is potentially sensitive to new physics. CDF has examined 75 pb^{-1} of dijet data and found no evidence for new physics. The CDF limits on a variety of processes are summarized in Figure 25. In particular, CDF has excluded an axigluon or coloron with a mass below $1.130 \text{ TeV}/c^2$ at 95% C.L.

7.4 Scalar Leptoquarks

Leptoquarks, as the name suggests, directly couple quarks to leptons and are predicted by Grand Unified Theories. In most models, leptoquarks are expected to couple only to fermions in the same generation because of experimental constraints from non-observation of flavor-changing neutral currents or helicity suppressed

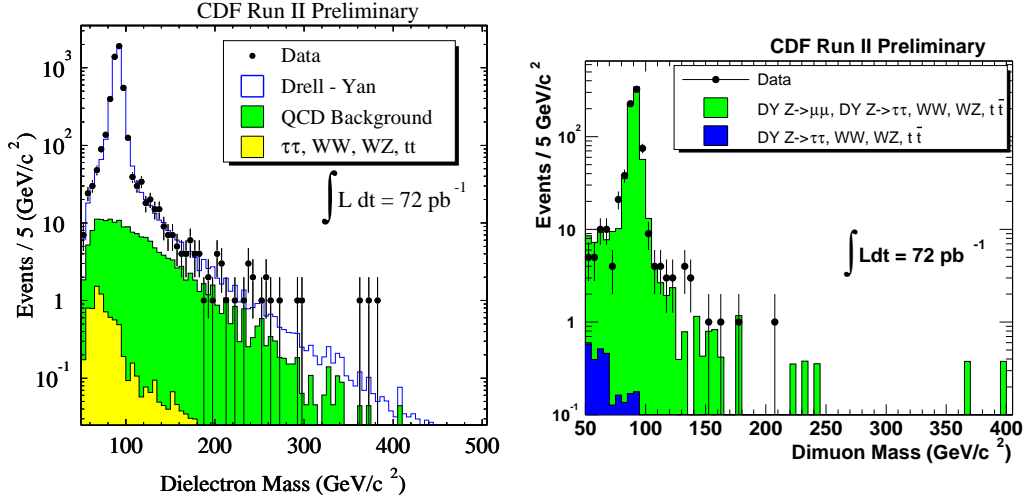


Figure 23: Measured dielectron (left) and dimuon (right) invariant mass distributions in 72 pb^{-1} of CDF data compared to the expectation from Standard Model processes.

decays. Leptoquarks are pair-produced at the Tevatron and the production cross-section has been calculated to NLO.³² Characteristic final states with isolated high p_T electrons or muons and energetic jets are produced by decays of pairs of first-generation leptoquarks ($eejj$, $ej\nu j$) and second-generation leptoquarks ($\mu\mu jj$ and $\mu j\nu j$), while the decays of third-generation leptoquarks ($\tau\tau jj$ and $\tau j\nu j$) are much harder to separate from the huge QCD multi-jet background. In addition, the jets+MET signature is sensitive to all three generations via the $\nu\nu jj$ final state.

The scalar sum of the transverse energies of the jets and muons from 100 pb^{-1} of D0 data is compared in Figure 26 to the expectation from the Standard Model and the signal from a second-generation leptoquark with a mass of $200 \text{ GeV}/c^2$. With 100 pb^{-1} of data, D0 sets limits of first generation $M(LQ) > 253 \text{ GeV}$ and second-generation $M(LQ) > 186 \text{ GeV}$ at 95% C.L. With 72 pb^{-1} of data, CDF sets limits of first-generation $M(LQ) > 230 \text{ GeV}$ at 95% C.L. and for all three generations $M(LQ) > 107 \text{ GeV}$ at 95% C.L. The CDF limits from the three different first-generation final states are also shown in Figure 26 as a function of the branching ratio $\beta = BR(LQ \rightarrow eq)$.

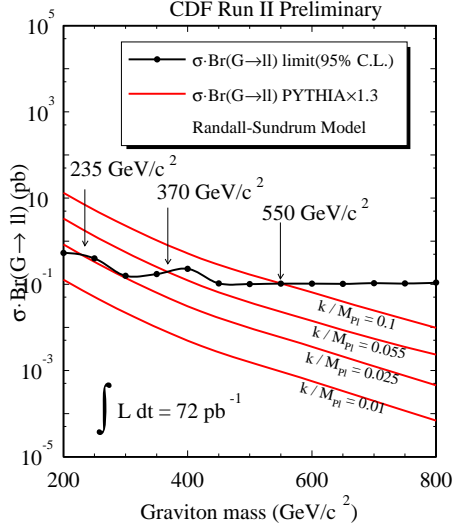


Figure 24: Limits on Randall-Sundrum graviton mass from 72 pb^{-1} of CDF dielectron and dimuon data.

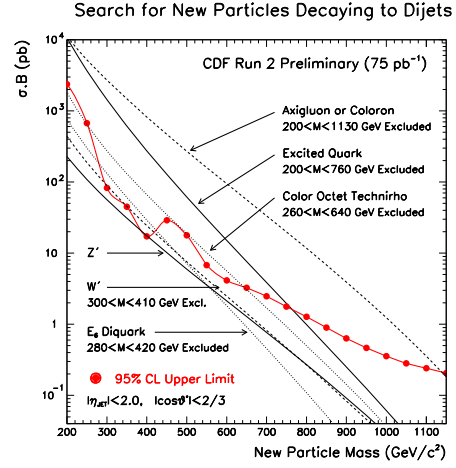


Figure 25: Limits from 75 pb^{-1} of CDF dijet data.

7.5 SUSY

Without a great deal of fine-tuning in the Standard Model, radiative corrections cause the Higgs boson mass to diverge quadratically. Supersymmetry is a symmetry that relates particles of different spin: each Standard Model particle has a SUSY partner differing by spin $\frac{1}{2}$ but with all other characteristics the same, including mass. At the cost of doubling the number of particles, supersymmetry automatically cancels the quadratic divergence in the Higgs boson mass[†]. In order to prevent violation of lepton and baryon conservation, an additional symmetry, called R-parity, is introduced, where $R=1$ for Standard Model particles and $R=-1$ for SUSY particles. R-parity conservation immediately implies that SUSY particles can only be produced in pairs and a SUSY particle will decay until the lightest SUSY particle is produced. This lightest SUSY particle, called the LSP, will be stable and is a good candidate for dark matter. Since there is no experimental evidence for any SUSY particles with the same mass as their Standard Model partners, SUSY must be a broken symmetry.

Except for a few specific cases, searches for SUSY at the Tevatron in Run II have not yet exceeded the limits set in Run 1 or by the LEP experiments. I will concentrate on the exceptions: searches for scalar top and scalar bottom by CDF,

[†]For other reasons, the SUSY Higgs sector actually has 5 physical Higgs particles.

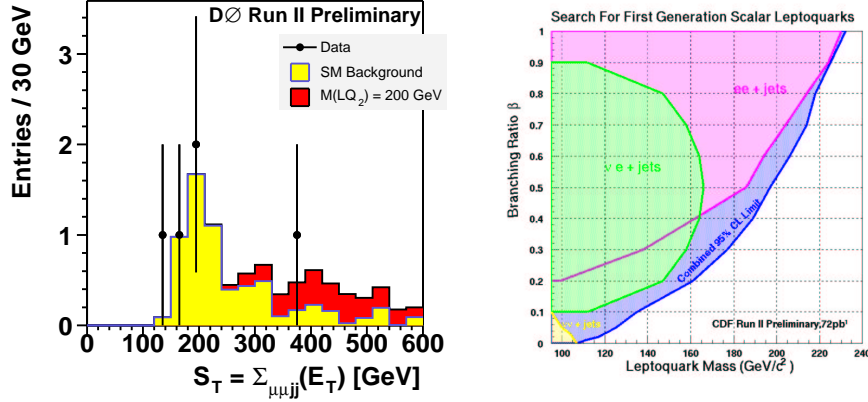


Figure 26: The measured scalar sum of the transverse energies in 100 pb^{-1} of D0 data compared to the expectation from Standard Model processes and a second-generation leptoquark with mass $200 \text{ GeV}/c^2$ (left). The combined limits from the CDF searches for a first-generation leptoquark with 72 pb^{-1} .

and searches for rare $B_s \rightarrow \mu^+ \mu^-$ decays by CDF and D0.

CDF performs a new search for massive stable charged particles by measuring the time-of-flight of high p_T tracks in a sample collected using a high p_T muon trigger. CHAMPS with a $\beta\gamma > 0.4$ are reconstructed efficiently by the pattern recognition of the tracking algorithm. The ionisation loss of the CHAMPS mean they leave signals in the muon chambers. A CHAMP will have an abnormally large time-of-flight, Δ_{TOF} , measured in the new time-of-flight detector. For track $p_T > 40 \text{ GeV}/c^2$ and $\Delta_{TOF} > 2.5 \text{ ns}$, CDF observes 7 events in 53 pb^{-1} . The expectation from background is $2.9 \pm 0.7(\text{stat}) \pm 3.1(\text{sys})$ events, where the systematic error is larger than the statistical error since it was extrapolated from a smaller control sample. The result of this search is completely model independent and can be easily interpreted within the context of a wide variety of models. The result is quantified in terms of a stable stop model since the strong production mechanism provides sufficient sensitivity for a significant measurement. Since no evidence for a signal is observed, CDF sets a limit of $m(\text{stop}) > 107 \text{ GeV}/c^2$ at 95% C.L. This surpasses the ALEPH limit³³ of $95 \text{ GeV}/c^2$ at 95% C.L.

The sbottom pair production cross-section is small compared to the gluino pair production cross section at the Tevatron. If the sbottom quark is lighter than the gluino, the dominant gluino decay is $\tilde{g} \rightarrow \tilde{b}_1 \bar{b}$ and the sbottom decays into $b\tilde{\chi}^0$. Therefore, gluino pair production, gives a very distinctive final state of 4 b -jets

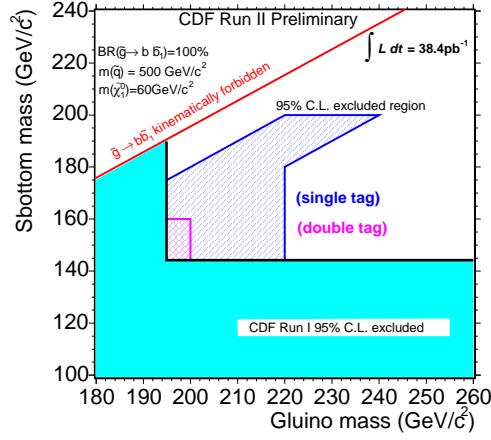


Figure 27: 95% C.L. contour exclusion in the gluino, sbottom mass plane as obtained by requiring a single SVX b-tag or a double SVX b-tag. The $\tilde{\chi}^0$ mass is assumed to be 60 GeV/c².

Experiment	BR	90% C.L.	95% C.L.
CDF	$BR(B_s \rightarrow \mu^+ \mu^-)$	9.5×10^{-7}	1.2×10^{-6}
D0	$BR(B_s \rightarrow \mu^+ \mu^-)$	1.6×10^{-6}	-
CDF	$BR(B_d \rightarrow \mu^+ \mu^-)$	2.5×10^{-7}	3.1×10^{-7}

Table 10: CDF and D0 search limits for $BR(B_s \rightarrow \mu^+ \mu^-)$ and $BR(B_d \rightarrow \mu^+ \mu^-)$.

and MET. CDF has performed a search for sbottom quarks from gluino decays in 38 pb^{-1} and the limits on the gluino and sbottom masses are shown in Figure 27.

The Standard Model prediction for the $BR(B_s \rightarrow \mu^+ \mu^-)$ is approximately 3.8×10^{-9} . However, various SUSY models predict an enhancement of this decay by a factor of 10 to 1000. In addition the BR increases as $\tan \beta$ increases, so this analysis has the potential to fill in the gap at high $\tan \beta$ from the loss in sensitivity due to the decreasing rate for the “golden” trilepton mode $\tilde{\chi}_1^+ \tilde{\chi}_2^0 \rightarrow W \tilde{\chi}_1^0 Z \tilde{\chi}_1^0 \rightarrow \ell \nu \tilde{\chi}_1^0 \ell \ell \tilde{\chi}_1^0$.

CDF and D0 have performed searches for $B_s \rightarrow \mu^+ \mu^-$ and $B_d \rightarrow \mu^+ \mu^-$ decays. In 113 pb^{-1} of data, CDF observes 1 candidate in the B_s and B_d search window, with an expected background of 0.54 ± 0.20 for B_s and 0.59 ± 0.22 for B_d . In 100 pb^{-1} of data, D0 observes 3 candidates in the B_s search window, with an expected background of 3.4 ± 0.8 . The limits are summarised in Table 10. CDF sets the world’s best limit of $BR(B_s \rightarrow \mu^+ \mu^-) < 1.2 \times 10^{-6}$ at 95% C.L. The B_d limits are not yet competitive with results from BABAR and BELLE.

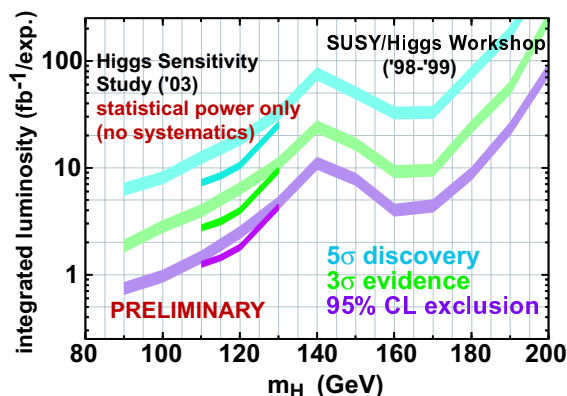


Figure 28: Integrated luminosities per experiment corresponding to the median expectations for 95% confidence level exclusion, 3σ evidence and 5σ discovery.

7.6 Standard Model Higgs Boson

Finding the Standard Model Higgs boson at the Tevatron is difficult - it requires the combination of the search results from all the possible decay channels by both experiments and a lot of data. Contrast this with the discovery of the top quark by CDF and D0, where each decay channel on each experiment had sufficient evidence with less than 100 pb^{-1} .

The region $m_H < 114.4\text{ GeV}/c^2$ is already excluded by the LEP experiments³⁴ at 95% C.L. At a mass of $115\text{ GeV}/c^2$, where ALEPH reported an excess compatible with the production of the Standard Model Higgs boson, the confidence $1 - CL_b$ of the combined LEP data expressing the level of consistency with the background hypothesis is 0.09, while the confidence CL_{s+b} measuring the consistency with the signal plus background hypothesis is slightly better at 0.15.

A recent study³⁵ of the sensitivity of CDF and D0 experiments to the Standard Model Higgs boson confirmed the findings of a previous 1998 study for m_H between 110 and $130\text{ GeV}/c^2$. The results of these studies are shown in Figure 28. For instance, with the 2000 pb^{-1} expected by 2007, there is a 50% probability to set a 95% C.L. limit of $m_H > 115\text{ GeV}/c^2$. With the expected integrated luminosity of $4000\text{--}9000\text{ pb}^{-1}$ by the end of Run II in 2009, the Tevatron may be able to increase the 95% C.L. limit set by LEP by $10\text{--}20\text{ GeV}/c^2$. However, the probability for a 5σ discovery is very low.

8 Conclusions

This review presents a snapshot of the physics results from the Tevatron experiments in summer 2003. CDF and D0 collected more data between spring 2002 and summer 2003 than during the entire previous run from 1989-1995. The first physics measurements with this new data are well underway: CDF has made the world's best measurements of the B_s and Λ_b masses; D0 has set the world's best limits on extra dimensions; both CDF and D0 have measured the top pair production cross-section. In the next year, with much more data and improved understanding of the upgraded detectors, you can expect to see a dramatic reduction in the statistical error and advances in beating down the systematic errors of these first results. More advanced measurements like the W boson mass and limit on the B_s mixing frequency will also appear at conferences soon. In the next few years, with the highest centre-of-mass energy in the world, CDF and D0 expect to set the world's best limits on the many theories beyond the Standard Model, or, maybe, find evidence for new physics!

9 Acknowledgements

I would like to thank all the CDF and D0 speakers at the EPS 2003 conference. I also profited greatly from the good advice of E. Barberis, K. Bloom, G. Brooijmans, C. Gerber, Y. Gershtein, R. Hughes, V. Jain, A. Juste, B. Klima, J. Kroll, J. Lewis, T. Liss, P. McNamara, M. Martinez-Perez, S. Rolli, R. Roser, M. Shapiro, M. Verzocchi, B. Winer and A. Yagil. Finally, I would like to thank SLAC for organising such a fascinating summer school.

References

- [1] CDF public web page <http://www-cdf.fnal.gov/>
- [2] D0 public web page <http://www-d0.fnal.gov/>
- [3] The European Physical Society Conference, 17-23 July 2003, Aachen, Germany. <http://eps2003.physik.rwth-aachen.de/index.php>
- [4] The XXI International Symposium on Lepton-Photon Interactions at High Energies, 11-16 August 2003, Fermilab, Batavia, Illinois, USA. <http://conferences.fnal.gov/lp2003/>
- [5] "The Run II handbook", <http://www-bd.fnal.gov/runII/index.html>

- [6] Talk by D. McGinnis at U.S. Department of Energy Review of Accelerator Run II.
<http://www-bd.fnal.gov/doereview03/>
- [7] B. Winstein and also N. Wright, these proceedings. C.I. Bennet *et al.*, arXiv:astro-ph/0302207.
- [8] CDF Collaboration, FERMILAB-Pub-96/390-E (1996).
- [9] D0 Collaboration, FERMILAB-PUB-96-357-E (1996).
- [10] S. Prell and also H. Aihara, these proceedings.
- [11] CDF collaboration, Phys. Rev. D68, 072004 (2003). hep-ex/0310043.
- [12] All world averages refer to those by the Particle Data Group, Phys. Rev. D66, 010001 (2002). See also <http://www-pdg.lbl.gov>
- [13] BABAR collaboration, Phys. Rev. D65, 091104 (2002).
- [14] CDF collaboration, Phys. Rev. Lett. 91, 241804 (2003). hep-ex/0307080.
- [15] M. Cacciari and P. Nason, JHEP 0309, 006 (2003).
- [16] BABAR Collaboration, Phys. Rev. Lett. 89, 281802 (2002).
- [17] P. Pinto, these proceedings.
- [18] W.J. Stirling *et al.*, Phys. Lett. B531 (2002) 216.
- [19] R. Hamberg *et al.*, Nucl. Phys. B359 (1991) 343.
- [20] S. Willenbrock, hep-ph/0211067.
- [21] E.H. Simmons, hep-ph/0211335.
- [22] M.L. Mangano *et al.*, hep-ph/0303085.
- [23] D0 Collaboration, Phys. Rev. Lett. 83, 1908 (1999).
- [24] CDF Collaboration, Phys. Rev. D64, 032002 (2001).
- [25] LEP Electroweak Working Group <http://lepewwg.web.cern.ch/LEPEWWG/>
- [26] M. Grunewald, hep-ex/0304023.
- [27] N. Arkani-Hamed, S. Dimopoulos, G. Dvali, Phys. Lett. B429, 263 (1998), hep-ph/9803315.
- [28] G. Giudice, R. Rattazzi and J. Wells, Nucl. Phys. B544, 3 (1999), hep-ph/9811291.
- [29] T. Han, J. Lykken and R. Zhang, Phys. Rev. D 59, 105006 (1999), hep-ph/9811350.
- [30] J. Hewett, Phys. Rev. Lett. 82, 4765 (1999).
- [31] L. Randall and R. Sundrum, Phys. Rev. Lett. 83, 3370 (1999) hep-ph/9905221 and Phys. Rev. Lett. 83, 4690 (1999) hep-th/9906064.
- [32] M. Kramer *et al.*, Phys. Rev. Lett. 79, 341, (1997).
- [33] ALEPH Collaboration, Phys. Lett. B537, 5 (2002).
- [34] ALEPH, DELPHI, L3 and OPAL collaborations and LEP Working Group for Higgs boson searches, Phys. Lett. B565:61-75, (2003), hep-ex/0306033.
- [35] CDF and D0 Collaborations, FERMILAB-PUB-03-320-E, October 2003.